

INVESTIGATION OF PHOSPHOLIPIDS IN ETHANOL AFFECTED PRENATAL MOUSE BRAIN USING DESI-MS IMAGING

Aafreen Kaur Bagga

A THESIS SUBMITTED TO
THE FACULTY OF GRADUATE STUDIES
IN PARTIAL FULFILLMENT OF THE REQUIREMENTS
FOR THE DEGREE OF
MASTER OF SCIENCE

GRADUATE PROGRAM IN CHEMISTRY
YORK UNIVERSITY
TORONTO, ONTARIO

December 2018

© Aafreen Kaur Bagga, 2018

Abstract

The prevalence of fetal alcohol spectrum disorder (FASD) is increasing exponentially due to the incognizant consumption of alcohol during early pregnancy. This research primarily focuses on monitoring the variation of phospholipid distribution in various regions of the brain using DESI-MS imaging. FASD mouse models were used in this study in which alcohol was administered to the pregnant mice during first trimester and 30 day old offsprings were chosen for the analysis. Principal component analysis was performed on six samples that illustrated enhanced level of PC(16:0/16:0), PC (16:0/18:1) throughout the brain; while the level of PE(P-16:0/22:6), PS(18:0/18:1), PS(18:0/20:0), PS(18:0/22:6), PI(18:0/20:4) and ST(24:1) increased specifically in the white matter of the brain in response to alcohol consumption. Conversely, alcohol reduced the level of PC(16:0/18:1), PE(P-18:0/22:6) and PC(18:0/18:1) exclusively in white matter of the brain. The changes noted in various phospholipids lay strong foundation for understanding alcohol mediated biochemistry in fetal brain development.

Acknowledgements

I would like to take this opportunity to thank those who were involved in my thesis research. My special thank you to my supervisor and mentor, Dr. Demian R. Ifa, for his fruitful advice throughout my journey as a graduate research student and for giving me a chance to be part of the center for research in mass spectrometry. A special thank you to Dr. Peter Carlen for his collaboration and assistance in animal husbandry section of this study. I am fortunate and grateful to Dr. Georg Zoidl and Dr. Gerald Audette for their continuous support and for providing immense guidance on neurobiological subject matters. Special thanks to Dr. Mark Bayfield for agreeing to be a part of my examination committee.

A cordial thank you to my colleague Consuelo Javiera Perez for patiently mentoring and training me on mass spectrometry, her knowledge and constant feedback was essential to my success. I would like to thank all my current and former colleagues and friends in Professor Ifa's research group: Amin Khatami, Shamina Prova, Maryam Yousefi Taemeh, Rachel Fu, and all the members of the Centre for Research in Mass Spectrometry. I would like to thank my dear colleague, Paige Whyte-Fagundes, for providing me immense support for initial sample preparation. Without her coordination, I could not have accomplished my research goals.

In the end I would like to thank my wonderful family for motivating and supporting me to pursue academia. My endurance, strength and perseverance are a mere reflection of yours.

Once again, thank you to all who took part in this memorable journey.

Table of Contents

Abstract	ii
Acknowledgements	iii
Table of Contents	iv
List of Tables	vi
List of Figures	vii
List of Abbreviations.....	xi
CHAPTER I	1
Introduction	1
1.1. Fetal Alcohol Spectrum Disorder	1
1.1.1. Ethanol migration to the fetus	1
1.1.2. Ethanol metabolism	2
1.2. Mouse Brain Structure and Function: Coronal Sections	4
1.3. Role of phospholipids in neuronal differentiation	6
1.4. FASD Investigation by Mass Spectrometry: Previous Work.....	8
1.5. Ambient Ionization Mass Spectrometry Imaging.....	9
1.5.1. Desorption Electrospray Ionization Mass Spectrometry (DESI-MS)	12
1.5.2. DESI-MS Imaging	15
1.6. Statistical Approach: Principal Component Analysis.....	16
1.7. Research Aims.....	17
CHAPTER II	19
Experimental.....	19
2.1. Mouse Husbandry and Ethanol Treatment	19
2.2. Mouse Brain Sample Preparation and Cryosectioning.....	19
2.3. Phospholipid Extraction and Characterization using HRMS.....	20
2.4. DESI-MS and DESI-MS Imaging.....	21

CHAPTER III	22
Results and Discussion	22
3.1. Phospholipid Identification by DESI-MS	22
3.2. Phospholipid Characterization by HRMS.....	26
3.3. DESI-MS Imaging.....	30
3.3.1. Principal Component Analysis in Positive Ionization Mode.....	32
3.3.2 Principal Component Analysis in Negative Ionization Mode	39
CHAPTER IV	46
Conclusion and Future Work	46
REFERENCES	48

List of Tables

Table 1: Phospholipid selectivity in lipid bilayers.	3
Table 2: Phospholipid ion characterization in positive ionization mode using ESI-HRMS.	27
Table 3: Phospholipid ion characterization in negative ionization mode using ESI coupled to LTQ-XL mass spectrometer.	28

List of Figures

- Figure 1:** Oxidative and non-oxidative metabolic pathways of ethanol..... 4
- Figure 2:** Anatomy of the mouse brain depicting localization of various substructures of the brain 5
- Figure 3:** Summary of various ambient ionization techniques with their respective mechanism of ionization, schematic of ion source and image resolution. Reproduced from Perez et. al.⁶⁰ 12
- Figure 4:** Conventional mass spectrometry techniques. (a) Matrix assisted laser desorption ionization (MALDI) shoots laser on sample embedded in matrix. (b) Desorption electrospray ionization (DESI) uses solvent spray to directly analyze samples (c) Secondary ion mass spectrometry (SIMS) uses pulsed ion beams to desorb molecules. Comparison of (d) spatial resolution (e) mass range capability, and (f) sample preparation requirement of MALDI, DESI and SIMS techniques. Adapted from reference.⁶² 13
- Figure 5:** Schematic of sample ionization by DESI-MS. Solvent is sprayed through the inner spray capillary (red) and nebulizing gas through the outer capillary (blue). Solvent hits the surface, ionizes molecules, and creates secondary charged droplets that enter into MS inlet.⁶⁴ 14
- Figure 6:** Schematic of (a) DESI geometric parameters with incident angle (α), collection angle (β), spray to surface distance (d_1), and MS inlet to surface distance (d_2). (b) DESI imaging that splits sample into multiple rows and acquires spectrum for each pixel within the row.^{67,68} 15
- Figure 7:** Full Scan DESI-MS spectra of (a) control mouse brain tissue in positive ion mode, (b) FASD mouse brain tissue in positive ion mode, (c) control mouse brain tissue in negative ion mode, (d) FASD mouse brain tissue in negative ion mode. Methanol was used as a spray solvent at 5 μ L/min flow rate. 22
- Figure 8:** Full Scan DESI-MS spectra in positive ionization mode. (a) MS spectrum corresponding to gray matter of healthy brain. (b) MS spectrum corresponding to white matter of healthy brain. (c) MS spectrum acquired in gray matter of FASD brain. (d) MS spectrum acquired in white matter of FASD brain. Methanol was used as a spray solvent at 5 μ L/min flow rate. 24
- Figure 9:** Full Scan DESI-MS spectra in negative ionization mode. (a) MS spectrum acquired in gray matter of healthy brain. (b) MS spectrum acquired in white matter of healthy brain. (c) MS spectrum corresponding to gray matter of FASD brain. (d) MS spectrum corresponding to white matter of FASD brain. Methanol was used as a spray solvent at 5 μ L/min flow rate. 25
- Figure 10:** Full Scan MS spectra of (a) mouse brain tissue section acquired by DESI-MS and (b) mouse brain lipid extract acquired by ESI-HRMS..... 26

Figure 11: ESI MS/MS spectra of phosphatidylcholine [PC(16:0/16:0) + Na]⁺ at m/z 756.5504 with its fragment ions (1) [PC(16:0/16:0) + Na - N(CH₃)₃]⁺ at m/z 697.4755; (2) [PC(16:0/16:0) + Na - C₅H₁₄NPO₄]⁺ at m/z 573.4837; (3) [PC(16:0/16:0) - Na - C₅H₁₄NPO₄]⁺ at m/z 551.5029; (4) [PC(16:0/16:0) + Na - C₁₅H₃₁COOH]⁺ at m/z 500.3104; (5) [PC(16:0/16:0) + Na - C₁₅H₃₁COOH - N(CH₃)₃]⁺ at m/z 441.2371. 27

Figure 12: ESI-HRMS spectra of control brain in positive ionization mode. (a) MS/MS Scan of molecule at m/z 772.5. (b) MS3 of ion (1) [PC(16:0/16:0)+K-N(CH₃)₃]⁺ at m/z 713.5 with fragment ions (2) [PC(16:0/16:0)+K-C₅H₁₄NPO₄]⁺ at m/z 589, and (3) [PC(16:0/16:0)-K-N(CH₃)₃]⁺ at m/z 551. (c) MS3 of ion (1) [PE(P-16:0/22:6)+Na-C₂H₅N]⁺ at m/z 729 with fragment ions (2) [PE(P-16:0/22:6)+Na-C₂H₈NPO₄]⁺ at m/z 631, (3) [PE(P-16:0/22:6)-Na-C₂H₈NPO₄]⁺ at m/z 609, (4) [PE(P-16:0/22:6)+Na-C₁₅H₃₂CHO-C₂H₅N]⁺ at m/z 488, (5) [PE(P-16:0/22:6)-Na-C₁₅H₃₂CHO-C₂H₅N]⁺ at m/z 463, and (6) [PE(P-16:0/22:6)+Na-C₂₁H₂₉COOH-C₂H₈NPO₄]⁺ at m/z 305. 30

Figure 13: DESI-MS images depicting phospholipid distribution in (a) control and (b) FASD brain sections of 30 day old mice acquired in positive ionization mode and (c) control and (d) FASD brain sections of 30 day old mice acquired in negative ionization mode. Images were collected at a resolution of 150 μm. 31

Figure 14: Principal Component Analysis score plot of FASD samples in positive ionization mode. Six mice samples including three wildtype (highlighted in green) and three FASD brain tissues (highlighted in pink) were subjected to PCA analysis. Principal component 1 and 2 (PC 1 and PC 2) corresponding to 44.7% and 22.9% variability in the data set were plotted on x and y axis respectively. The dataset was normalized to the base peak at m/z 798. PCA analysis was executed on 16 ions corresponding to entire brain ROI using 5% to 8% relative intensity threshold selection criteria. 33

Figure 15: Principal Component Analysis of FASD samples in positive ionization mode. PCA analysis was computed using entire brain area selected as the region of interest. Six mice samples comprising three wildtype (green) and three FASD (pink) brain tissues were subjected to PCA analysis. Principal component 1 and 2 (PC1 and PC2) corresponding to 58.1% and 35.8% variability in the data set were plotted on x-axis and y-axis respectively. The dataset was normalized to the base peak at m/z 798. (a) PCA score plot with wildtype (WT) and FASD objects representing average mass spectrum obtained from whole brain ROI of each sample. (b) PCA biplot indicates contribution of various phospholipid ions in the separation of FASD and wildtype tissue samples. The ions at m/z 782 and m/z 826 formed acute angle with wildtype cluster and were consequently more abundant in wildtype brains. While, the ions at m/z 756 and m/z 772 formed acute angle with the FASD cluster and were consequently more abundant in FASD brains. 34

Figure 16: Principal Component Analysis of FASD samples in positive ionization mode. PCA analysis was conducted on gray (pink) and white matter (green) ROI. Principal component 1 and 2 (PC1 and PC2) corresponding to 94.6% and 4.7% variability in the data set were plotted on x-axis and y-axis respectively. The dataset was normalized to the base peak at m/z 782. (a) PCA

score plot include objects depicting average mass spectrum obtained from respective ROI of each sample. (b) PCA biplot indicates contribution of various phospholipid ions in the separation of gray and white matter of FASD tissue samples. The ion at m/z 756 formed acute angle with the cluster of gray matter and was consequently more abundant in the gray matter as opposed to the white matter of FASD brains. All other ions formed acute angle with the cluster of white matter and were consequently more abundant in the white matter of FASD brains..... 35

Figure 17: Principal Component Analysis of wildtype samples in positive ionization mode. PCA analysis was performed on region of interest corresponding to gray (pink) and white (green) matter of healthy brain. Principal component 1 and 2 (PC1 and PC2) corresponding to 87.1% and 8.7% variability in the data set were plotted on x-axis and y-axis respectively. The dataset was normalized to the base peak at m/z 798. (a) PCA score plot include points representing average mass spectrum of each sample obtained from its respective ROI. (b) PCA biplot shows contribution of various phospholipid ions in the separation of gray and white matter of healthy mouse brain samples. The ion at m/z 826 formed acute angle with the cluster of white matter and was consequently more abundant in the white matter as opposed to the gray matter of healthy brains. All other ions formed acute angle with the cluster of gray matter and were consequently more abundant in the gray matter of healthy brains. 36

Figure 18: Principal Component Analysis of gray matter ROI in FASD (pink) and healthy (green) tissue samples in positive ionization mode. Principal component 1 and 2 (PC1 and PC2) corresponding to 73.8% and 20.7% variability in the data set were plotted on x-axis and y-axis respectively. The dataset was normalized to the base peak at m/z 782. (a) PCA score plot exhibit objects associated with average mass spectrum obtained from respective ROI of each sample. (b) PCA biplot shows contribution of different phospholipid ions in the gray matter of FASD and healthy mouse brain samples. The ion at m/z 756 formed acute angle with FASD cluster and was consequently more abundant in gray matter of FASD brains. All other ions formed acute angle with the wildtype cluster and were consequently more abundant in the gray matter of healthy brains..... 37

Figure 19: Principal Component Analysis of ROI corresponding to white matter of FASD (pink) and healthy (green) brain samples in positive ionization mode. Principal component 1 and 2 (PC1 and PC2) corresponding to 51% and 40.6% variability in the data set were plotted on x-axis and y-axis respectively. The dataset was normalized to the base peak at m/z 798. (a) PCA score plot include objects representing average mass spectrum obtained from white matter ROI of each sample. (b) PCA biplot shows contribution of five major phospholipid ions in the white matter of FASD and wildtype samples. All the ions formed acute angle with FASD cluster were consequently more abundant in the white matter of FASD brains..... 38

Figure 20: Principal Component Analysis of FASD samples in negative ionization mode. Six mice samples comprising three wildtype (green) and three FASD (pink) brain tissues were subjected to PCA analysis. PCA analysis was computed using entire brain area selected as the region of interest. Principal component 1 and 2 (PC1 and PC2) corresponding to 87.2% and 9.6% variability in the data set were plotted on x-axis and y-axis respectively. The dataset was

normalized to the base peak at m/z 834. (a) PCA score plot shows wildtype and FASD objects corresponding to the average mass spectrum obtained from whole brain ROI of each sample. (b) PCA biplot indicates contribution of 5 major phospholipid ions in the separation of FASD and wildtype tissue samples. All the ions formed acute angle with FASD cluster and were consequently more abundant in the entire FASD brain in comparison to the healthy brain. 40

Figure 21: Principal Component Analysis of wildtype samples in negative ionization mode. PCA analysis was performed on region of interest corresponding to gray (pink) and white (green) matter of healthy brain. Principal component 1 and 2 (PC1 and PC2) corresponding to 98.2% and 2.4% variability in the data set were plotted on x-axis and y-axis respectively. The dataset was normalized to the base peak at m/z 834. (a) PCA score plot include points representing average mass spectrum of each sample obtained from its respective ROI. (b) PCA biplot shows contribution of different phospholipid ions in the separation of gray and white matter of healthy mouse brain samples. All the ions formed acute angle with the cluster of white matter and were consequently more abundant in the white matter of healthy brains. 41

Figure 22: Principal Component Analysis of FASD samples in negative ionization mode. PCA analysis was conducted on gray (pink) and white (green) matter ROI. Principal component 1 and 2 (PC1 and PC2) corresponding to 96.9% and 2.7% variability in the data set were plotted on x-axis and y-axis respectively. The dataset was normalized to the base peak at m/z 834. (a) PCA score plot include objects depicting average mass spectrum obtained from respective ROI of each sample. (b) PCA biplot indicates contribution of various phospholipid ions in the separation of gray and white matter of FASD tissue samples. All the ions formed acute angle with the cluster of white matter and were consequently more abundant in the white matter of FASD brains. 42

Figure 23: Principal Component Analysis of ROI corresponding to gray matter of FASD (pink) and healthy (green) tissue samples in negative ionization mode. Principal component 1 and 2 (PC1 and PC2) corresponding to 95.3% and 2.9% variability in the data set were plotted on x-axis and y-axis respectively. The dataset was normalized to the base peak at m/z 834. (a) PCA score plot exhibit objects associated with average mass spectrum obtained from respective ROI of each sample. (b) PCA biplot shows contribution of different phospholipid ions in the gray matter of FASD and healthy mouse brain samples. All the ions formed acute angle with the FASD cluster and were consequently more abundant in the gray matter of FASD brains. 43

Figure 24: Principal Component Analysis of ROI corresponding to white matter of FASD (pink) and healthy (green) brain samples in negative ionization mode. Principal component 1 and 2 (PC1 and PC2) corresponding to 87.9% and 9.6% variability in the data set were plotted on x-axis and y-axis respectively. The dataset was normalized to the base peak at m/z 788. (a) PCA score plot include objects representing average mass spectrum obtained from white matter ROI of each sample. (b) PCA biplot shows contribution of various phospholipid ions in the white matter of FASD and wildtype samples. All the ions formed acute angle with the FASD cluster and were consequently more abundant in the white matter of FASD brains. 44

List of Abbreviations

ADH	Alcohol Dehydrogenase
AFP	Alpha Fetoprotein
AGC	Automatic Gain Control
AKT	Protein Kinase B
ALDH	Aldehyde Dehydrogenase
AMS	Ambient Ionization Mass Spectrometry
ATP	Adenosine Triphosphate
BBB	Blood Brain Barrier
CMC	Carboxymethylcellulose
CNS	Central Nervous System
CYP2E1	Cytochrome P450 2E1
DESI	Desorption Electrospray Ionization
DHA	Docosahexaenoic Acid
DNA	Deoxyribonucleic Acid
ESI	Electrospray Ionization
FAEE	Fatty Acid Ethyl Ester
FASD	Fetal Alcohol Spectrum Disorder
GD	Gestation Day
HRMS	High Resolution Mass Spectrometry
HS-SPME	Headspace Solid Phase Microextraction
LC	Liquid Chromatography
MAE	Microwave Assisted Extraction
MALDI	Matrix Assisted Laser Desorption Ionization
MRI	Magnetic Resonance Imaging
MS	Mass Spectrometer
MSI	Mass Spectrometry Imaging
NaCl	Sodium Chloride
PAE	Prenatal Alcohol Exposure
PC	Phosphatidylcholine

PCA	Principal Component Analysis
PE	Phosphatidylethanolamine
PEth	Phosphatidylethanol
PI	Phosphatidylinositol
PS	Phosphatidylserine
ROI	Region of Interest
SIMS	Secondary Ion Mass Spectrometry
S/N	Signal to Noise Ratio
ST	Sulfatide
TOF	Time of Flight
USTDL	United States Drug Testing Laboratory
UV	Ultraviolet
WT	Wildtype

CHAPTER I

Introduction

1.1. Fetal Alcohol Spectrum Disorder

Fetal Alcohol Spectrum Disorder (FASD) is a broad term for diseases that encompass psychological, behavioral and neurobiological deficits resulting from alcohol consumption during pregnancy. FASD is most prevalent in South-African communities with 135-207 FASD cases per 1,000 births while the prevalence rate varies from 2.3% to 6.3% of the newly born children in developed countries.¹ The extent of fetal damage due to ethanol exposure depends on couple of factors including the timing, dose and frequency of ethanol consumed.² The impact of environmental agents on brain development is as critical as the genetic factors since constituents of vittles consumed by expectant mother can be transported to fetus.³ Alcohol is one of the environmental agents that has been shown to cause significant growth deficits in the fetus. It can result in facial dysmorphology and can also hinder the growth of central nervous system (CNS). Children afflicted by FASD are likely to have short palpebral fissures, smooth philtrum and thin upper lip.^{4,5} FASD can also result in reduced brain size and volume.⁶ MRI studies have demonstrated underdevelopment of specific brain areas such as hippocampus, cerebellum, basal ganglia, caudate nucleus, frontal lobe, and corpus callosum which causes impairment in learning, reading, memory, coordination, and psychological functioning.^{6,7} On the other hand, cortex has been found to be greater in thickness with atypical patterns of pruning and myelination that may obstruct neural connections.^{6,8}

1.1.1. Ethanol migration to the fetus

Ethanol consumed by the expectant women can directly impact the developing fetus as ethanol, being small uncharged polar molecule, has the ability to rapidly diffuse through lipid membrane and merge into fetal blood through placenta.⁹ Ethanol can also cross the blood brain

barrier (BBB) and impair the growth of neurons along with disrupting critical signaling pathways essential for brain maturation. Furthermore, presence of ethanol in placenta prompts umbilical cord to vasoconstrict in an attempt to reduce the transport of ethanol to the fetus. However, vasoconstriction also reduces the migration of oxygen and other essential nutrients to the fetus that in turn effects the development of CNS.^{10,11} Once ethanol enters the fetal blood stream, it can be metabolized by numerous enzymes through oxidative and non-oxidative pathways.

1.1.2. Ethanol metabolism

In mammals, metabolism of ethanol via oxidative pathway includes alcohol dehydrogenase (ADH) and cytochrome P450 2E1 (CYP2E1) enzymes that transform ethanol to acetaldehyde followed by aldehyde dehydrogenase (ALDH) that catalyzes acetaldehyde to acetate in mitochondria (Figure 1). Previous studies have demonstrated the presence of both ADH and ALDH in the fetus while activity of these enzymes have been shown to be significantly low in comparison to the adult.^{10,12} Consequently, ethanol metabolic intermediates accumulate in the fetal body and impair neuronal survival and proliferation, mitochondrial function, ATP production, membrane integrity and neurotransmitter function.¹³

Acetaldehyde accumulates in the body when rate of ethanol consumption is greater than the rate of ethanol metabolism as well as when ethanol metabolic pathway slows down in the case of genetic variations persisting in ALDH2.^{10,13} Acetaldehyde, being electrophilic in nature, reacts rapidly with lipids, proteins and DNA; thereby impairing lipid and protein function, as well as promoting DNA damage.¹³ Acetaldehyde can alter membrane fatty acid and phospholipid profiles causing changes in membrane permeability, diffusion, fluidity, as well as reducing the activity of certain enzymes that affect overall cell function and integrity.^{9,10,14,15} Phospholipids distribute assymmetrically within the lipid bilayer membrane such that neutral zwitterionic phospholipids with large polar head groups align towards the exofacial leaflet while neutral or acidic phospholipids with small polar head groups orient towards the cytofacial leaflet (Table 1). Such phospholipid distribution prompts cytofacial leaflet to be more negatively

charged than the exofacial leaflet establishing a charge gradient across the phospholipid membrane. The movement of phospholipids within the plane of the membrane is easily attainable and it does not disrupt the charge gradient. Conversely, the transbilayer migration that entails the movement of lipids from exofacial leaflet to cytofacial leaflet or vice versa is relatively intricate as it requires the passage of lipids through the hydrophobic bilayer core which has high activation energy associated with it.¹⁴ Ethanol has been shown to increase the rate of transbilayer migration in the synaptosome that interferes with the electrophysiology of the plasma membrane as well as intracellular signaling caused by the release of cytofacially bound divalent metal counterions.^{9,14} ALDH can diminish the teratogenic effects of acetaldehyde by reducing acetaldehyde to acetate which ultimately gets converted to carbon dioxide and water via the Krebs cycle.¹⁶

Table 1: Phospholipid selectivity in lipid bilayers.

Leaflet	Lipid Enriched	Charge
Exofacial	Phosphatidylcholine	Zwitterionic
	Sphingomyelin	Zwitterionic
	Glycolipids	Neutral or anionic
Cytofacial	Phosphatidylserine	Anionic
	Phosphatidylinositol	Anionic
	Phosphatidylethanolamine	Neutral
	Cholesterol	

Alcohol can also be metabolized via non-oxidative pathways by fatty acid ethyl ester (FAEE) synthase and phospholipase D (Figure 1). FAEE synthase esterifies fatty acid in the presence of ethanol forming fatty acid ethyl ester while phospholipase D utilizes ethanol as a substrate to convert phosphatidylcholine to phosphatidylethanol (PEth) via transphosphatidyl transfer reaction. In normal conditions, phospholipase D hydrolyzes phospholipids leading to the formation of phosphatidic acid; however, in the presence of ethanol, ethanol competes with water for phospholipase D resulting in the accumulation of phosphatidylethanol that disrupts the surface charge and lipid profile of the membrane together with the distortion of electrostatic interactions and hydrogen bonds persisting

between the lipids. Ethanol also interferes with phospholipase D mediated signal transduction by reducing the production of phosphatidic acid required for optimum cellular activity.¹⁷

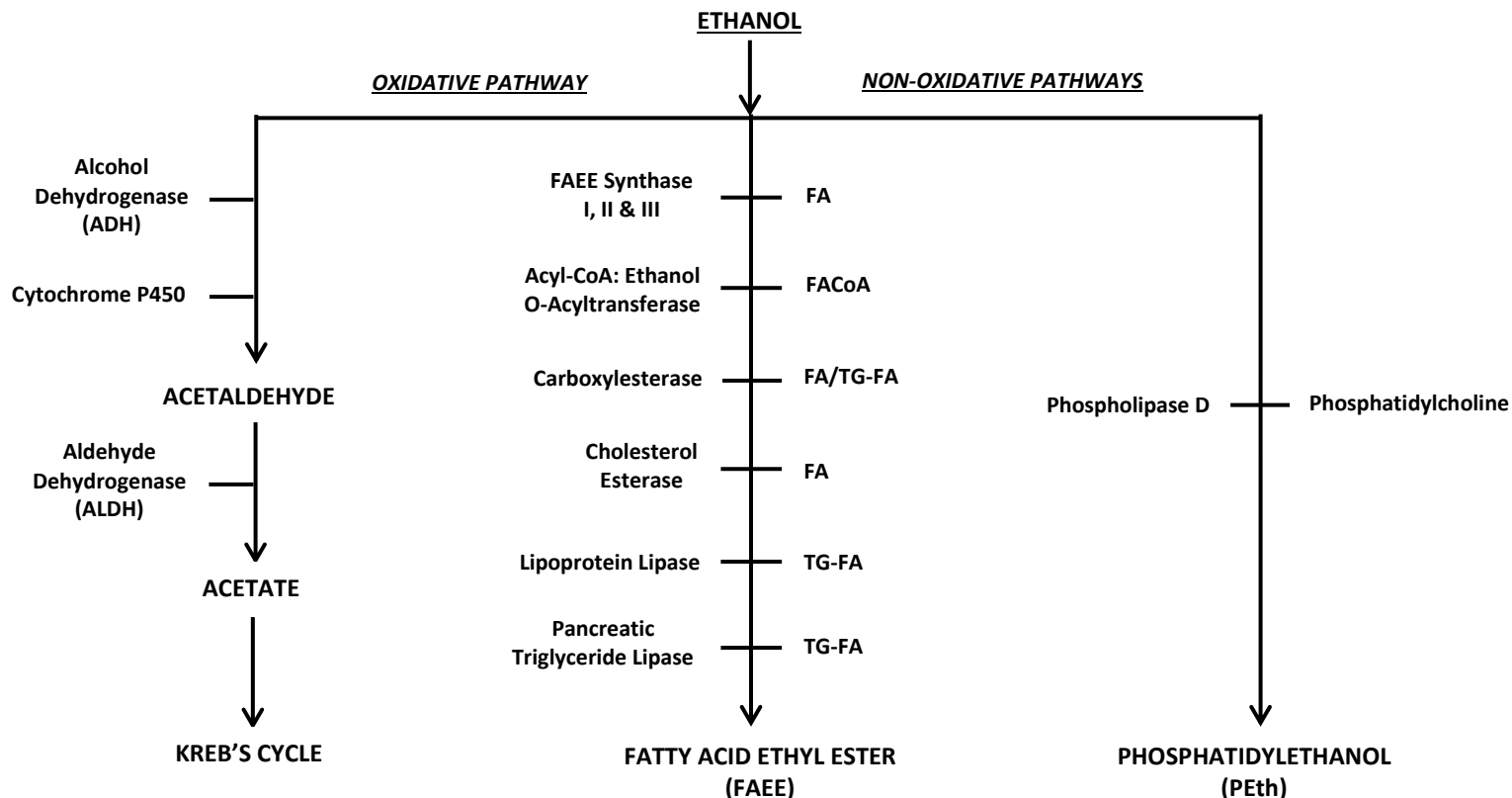


Figure 1: Oxidative and non-oxidative metabolic pathways of ethanol.

1.2. Mouse Brain Structure and Function: Coronal Sections

Brain is one of the most important organs of our body that processes received signals and controls our functions such as emotions, intelligence, creativity and memory. Some of the critical substructures of the brain are cerebral cortex, corpus callosum, hippocampus, thalamus, and hypothalamus whose localization is illustrated in Figure 2. Cerebral cortex includes visual cortex, auditory cortex, somatosensory cortex, and motor cortex. Cortex primarily contains nerve cell bodies that makes it appear as gray-brown; thereby giving it a name – gray matter. The inferior border of the cerebral cortex can be identified in the sagittal view as the superior border of the corpus callosum.¹⁸ Cerebral cortex is primarily responsible for motor functions, as

well as language, learning, attention and mental imagery.¹⁹ Corpus callosum contains large number of axons that makes its appearance white; thereby giving it a name – white matter. It is located throughout the cerebrum and forms distinct M shaped structure.¹⁸ It interconnects the two hemispheres and transmits messages from one side of the brain to the same region on the other side of the brain.²⁰

Hippocampus is located at the immediate inferior and medial-lateral to the corpus callosum. Hippocampus regions belonging to the left and right hemispheres are separated by lateral ventricles and are connected via neurons.¹⁸ Hippocampus is part of the limbic system and is responsible for consolidating information from short term memory to long term memory.²¹ Hypothalamus spans from the midline to interior clefts in both hemispheres and primarily controls autonomic system.¹⁸ It plays critical roles in controlling behaviors such as hunger, thirst and sleep, as well as in maintaining homeostasis such as regulating body temperature, blood pressure, emotions and secretion of hormones.²² Thalamus is located superior to hypothalamus and is surrounded by third ventricles.¹⁸ It relays sensory signals, including motor signals, to the cerebral cortex. It plays a role in the regulation of pain sensation, consciousness, sleep, attention, alertness, and memory.²³

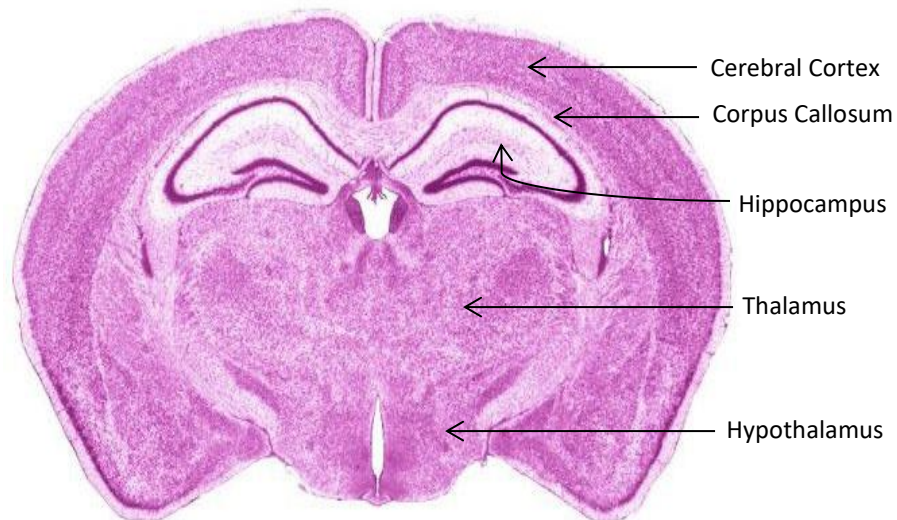


Figure 2: Anatomy of the mouse brain depicting localization of various substructures of the brain

1.3. Role of phospholipids in neuronal differentiation

Neuronal differentiation is a complex process that initiates with the formation of neurites, long cellular projections, from the cell body. These neurites undergo extensive changes in length and shape during its elongation stage to reach a specific target.²⁴ Neuronal outgrowth dramatically increases cell surface area which is mediated by different types of phospholipids involved in membrane biosynthesis. Membranes play critical role in the generation and propagation of ionic currents essential for neuronal signal transduction.²⁵ Among various phospholipids involved in membrane biosynthesis, phosphatidylcholine (PC) being the most abundant phospholipid accounts for about 58% of total phospholipids in neuronal membranes.²⁶ Furthermore, PC plays critical role in the synthesis of an essential neurotransmitter, acetylcholine, which modulates synaptic transmission and excites various classes of neurons such as pyramidal cells and dendrite-targeting GABAergic interneurons.²⁷ The reduction of PC level is associated with memory deficits in dementia and Alzheimer diseased states.^{28,29} In these diseased states, increasing the level of acetylcholine specifically in the cortical region have demonstrated enhanced neuron sensitivity to external stimuli and increased focused attention to sensory input.³⁰ On the other hand, extensive accumulation of PC in the brain is also detrimental and is linked to conditions such as schizophrenia. Schizophrenia patients demonstrate higher levels of acetylcholine that causes overstimulation of nicotinic and muscarinic receptors at the synapses.^{30,31} Furthermore, acetylcholinesterase knockdown study revealed increased anxiety and depression like symptoms associated with excessive acetylcholine accumulation in rodents.³²

Phosphatidylserine (PS) is the major anionic phospholipid that accounts for 13-15% of phospholipids in the cerebral cortex. PS is predominantly localized in the inner leaflet of the plasma membrane; however, it is initially introduced in the exofacial leaflet of the membrane and is then migrated to cytofacial leaflet by floppase enzyme with the aid of ATP.³³ Excessive accumulation of PS in neuronal cells increases its buildup in the outer leaflet causing uncontrolled ion fluxes across the membrane that consequently disrupts cellular signalling.³⁴ Furthermore, the accretion of PS in outer leaflet triggers apoptotic responses in the cell via

phagocytosis causing neuronal degeneration.^{35,36} Within the cytofacial leaflet, PS plays critical role in the release of neurotransmitters by exocytosis and modulation of numerous synaptic receptors and proteins in neuronal membranes.³⁷ PS facilitates neuronal differentiation and survival by activating signaling pathways mediated by various proteins including Akt, protein kinase C and Raf-1 that interacts directly with the anionic domain of PS.³⁷ DHA has demonstrated to enhance PS production in neuronal membranes; thereby facilitating PS associated signaling mechanisms. However, alcohol have been shown to inhibit DHA induced PS production pathway imposing adverse effects on critical signalling mechanisms involved in neuronal differentiation.³⁷

Phosphatidylinositol is one of the most reactive phospholipids due to its inositol ring constituting multiple free hydroxyl groups.³⁸ These hydroxyl groups can be phosphorylated in a combinatorial manner by PI kinases forming astonishing range of inositol phosphates with unique functions.³⁹ Phosphorylated head groups of PI mediates recruitment of proteins to the membrane which is essential for various cellular pathways including cell proliferation and survival, vesicle trafficking, ion channel regulation, and glucose transport.⁴⁰ Amplified PI levels in the brain can increase the abundance of its phosphorylated products that can ultimately overstimulate critical cellular pathways causing adverse effects related to brain development. Such adverse effects have been recognized in cancer patients where enhanced PI 3-kinase activity excessively activates cell proliferation pathways. PI 3-kinase inhibitors have been proposed as promising drug candidates for cancer therapies.⁴¹

Sulfatide is the most abundant sulfoglycolipid that is enriched in myelin sheath and accounts for about one-third of total myelin lipids.⁴² Sulfatide (ST) is present in oligodendrocytes and Schwann cells in early stages of development and is upregulated before the progression of myelination.⁴³ ST is primarily located in the outer leaflet of the membrane and constitutes about two-third of the phospholipids present exclusively in the exofacial leaflet. ST is responsible for the differentiation of myelinating cells,⁴⁴ and formation of paranodal junction by acting as a negative regulator of oligodendrocyte differentiation such that its

deficiency causes increase in the number of differentiated oligodendrocytes in the brain.^{45,46} ST also plays critical role in glial axon signaling by maintaining sodium and potassium ion channel clusters.⁴³ The excessive accumulation of ST in neurons can lead to axonal degeneration, demyelination and cortical hyperexcitability causing significant impairments in brain development.^{47,48} One of the diseases associated with sulfatide accumulation is metachromatic leukodystrophy that has been shown to reduce nerve conduction velocity, increase heterogeneity in the thickness of myelin, and upregulate frequency of hypomyelinated and demyelinated axons in corpus callosum of afflicted patients.⁴⁷ Patients suffering from Parkinson's disease also demonstrate elevated levels of ST in superior frontal and cerebellar gray matter.⁴⁹ Furthermore, lethal audiogenic seizures have been shown to result due to excessive ST accumulation in mouse neurons.⁵⁰

1.4. FASD Investigation by Mass Spectrometry: Previous Work

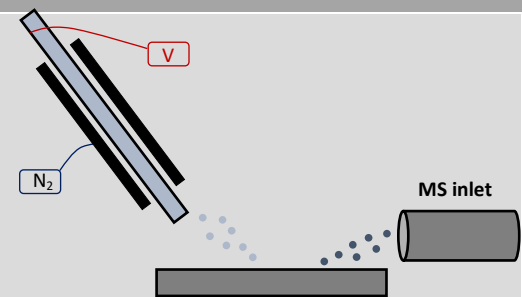
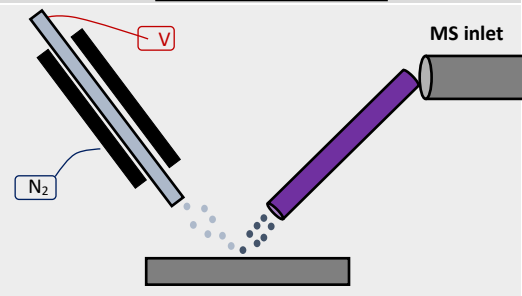
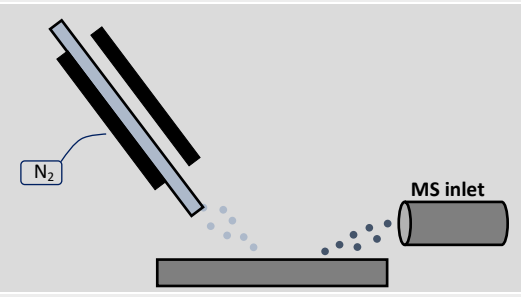
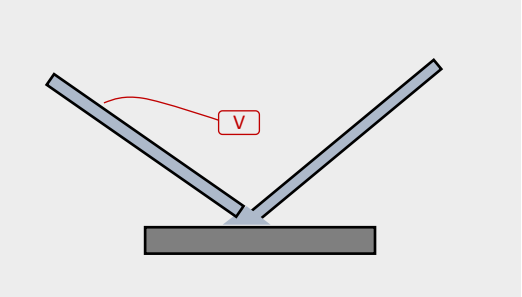
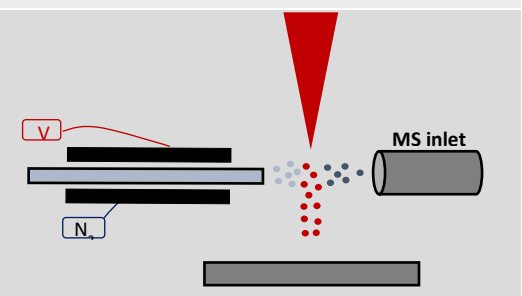
Over the last decade, FASD research by mass spectrometry increased immensely and has been directed towards the detection of non-oxidative ethanol metabolites, FAEE and PEt, and the development of new protein biomarkers for FASD identification. Various MS based methods were developed and validated to quantify FAEE in neonatal meconium and hair matrices with high accuracy and precision. FAEEs were isolated by headspace solid phase microextraction (HS-SPME)⁵¹ and microwave assisted extraction (MAE)⁵² methods, which were detected by GC-MS or LC-MS techniques⁵³ and quantified using D5-ethyl ester internal standards. The detection method of PEt, another ethanol metabolic product, was recently developed by the United States Drug Testing Laboratory (USTDL) in dried blood spots that were collected from newborns for routine testing and illicit drug testing.⁵⁴ PEt were isolated by ultrasound assisted dispersive liquid-liquid microextraction and detected by LC-MS.⁵⁵

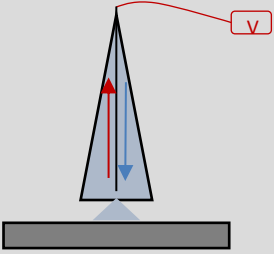
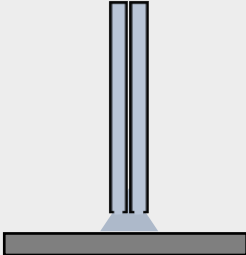
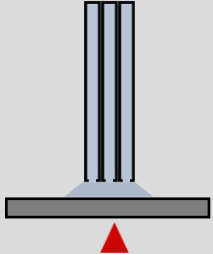
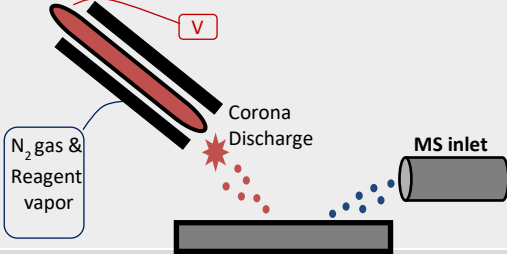
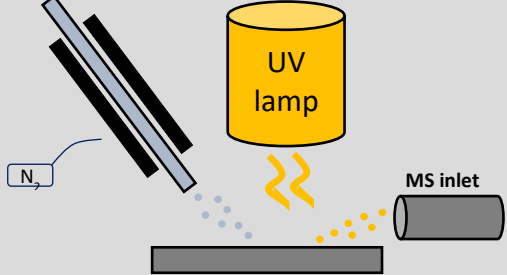
The effect of ethanol on placental, embryonic, endothelial and amniotic fluid protein expression was also explored during recent years using MS based techniques. Forty-five Placental proteins were detected by Q Exactive Hybrid Quadrupole-Orbitrap mass spectrometer

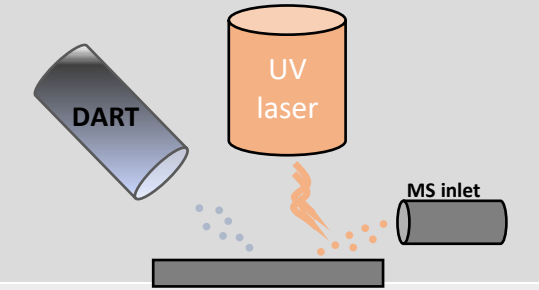
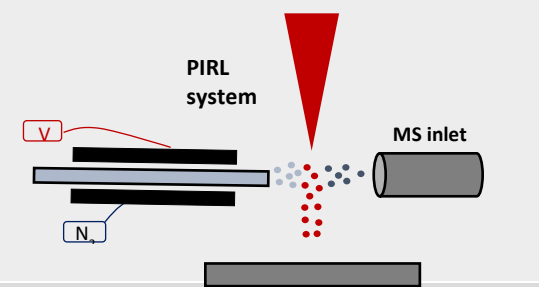
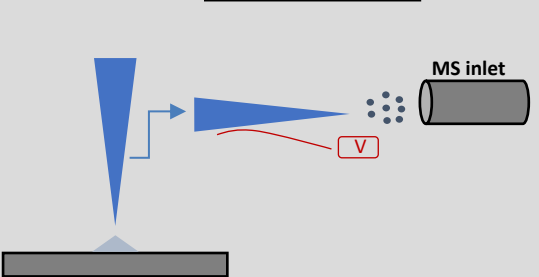
that were found to be related to alcohol metabolism. Additionally, specific isoforms of alcohol dehydrogenase and aldehyde dehydrogenase were discovered to be altered in response to ethanol.⁵⁶ Similarly, modification in 40 embryonic proteins involved in cellular function, ubiquitin proteasome pathway and Myc transcription factor cascades were identified using LC-MS.⁵⁷ The endothelial proteome was also investigated using iTRAQ labeling followed by LC-MS analysis; fourteen proteins were discerned to be upregulated while 17 proteins were downregulated including those responsible for transcription/translation regulation, histones and redox balance.⁵⁸ Lastly, amniotic fluid proteome analysis conducted by matrix assisted laser desorption-time of flight (MALDI-TOF) mass spectrometry exhibited significant drop in alpha fetoprotein (AFP) levels which can be used as a potential biomarker for the identification of FASD.⁵⁹ To the best of our knowledge, DESI-MS has not been employed to inspect FASD phospholipids till date and will thus be the primary goal of this study.

1.5. Ambient Ionization Mass Spectrometry Imaging

Mass spectrometry imaging (MSI) allows chemical and spatial profiling of analytes in a wide variety of sample types with complex matrices. Ambient ionization mass spectrometry (AMS) imaging is a specific field of MSI that enables the acquisition of sample images in an open environment. One of the major benefits associated with AMS methods is that the sample requires little or no sample preparation and can be analyzed directly in the native state thereby reducing total time of analysis. Furthermore, pre-treatment of the sample can be accomplished concurrently during imaging analysis which cannot be achieved in vacuum based methods. AMS has been widely explored in numerous areas of research including forensics, drug development and discovery, lipidomics, metabolomics, cancer diagnostics, microbiology, and natural product analysis. Cancer and disease diagnostics is predominantly accomplished by histopathology analysis that utilizes various staining procedures followed by microscopic analysis. However, AMS is rapidly gaining recognition due to its ability to detect multiple biomarkers in a single analysis with significantly shorter analysis time in comparison to histopathology tests. Since the invention of desorption electrospray ionization, about 40 unique AMS ionization technique have been developed, some of which are summarized in Figure 3.

Ambient Ionization Technique	Type of Ionization	Ion Source Schematic	Imaging Resolutions
Desorption Electro spray Ionization (DESI)	Liquid extraction		100-200 μm (35 μm) ^a
Air Flow Assisted Desorption Electro spray Ionization (AFADESI)	Liquid extraction		200-300 μm (200 μm) ^a
Easy Ambient Sonic-Spray Ionization (EASI)	Spray based		100-200 μm (50 μm) ^a
Nano Electro spray Desorption Ionization (nano-DESI)	Liquid Extraction		50-100 μm (12.5 μm) ^a
Laser Ablation Electro spray Ionization (LAESI) ¹⁴ / Laser Electro spray Mass Spectrometry (LEMS)	Two steps (Laser ablation and Electro spray ionization)		200-300 μm (30 μm) ^a / 60 μm ^a

Ambient Ionization Technique	Type of Ionization	Ion Source Schematic	Imaging Resolutions
Single Probe (SP)	Liquid Extraction		10-20 μm (8.5 μm) ^a
Liquid Microjunction-Surface Sampling Probe (LMJ-SSP)	Liquid Extraction		0.5-1 mm (0.5 mm) ^a
Laser Ablation-Liquid Capture Surface Analysis (LA-LCSA)	Liquid Extraction		(50 μm) ^a
Desorption Atmospheric Pressure Chemical Ionization (DAPCI)	Plasma		200-500 μm (58 μm) ^a
Desorption Atmospheric Pressure Photoionization (DAPPI)	Photo-ionization		1000 μm (700 μm) ^a

Ambient Ionization Technique	Type of Ionization	Ion Source Schematic	Imaging Resolutions
Laser Ablation Direct Analysis in Real Time Imaging (LADI)	Two step (Laser Ablation and Plasma Ionization)		50 μm^a
Picosecond Infrared-Laser Ablation Electro spray Ionization (PIR-LAESI)	Two step- (Laser Ablation and electro spray ionization)		100 μm^a
Liquid Extraction Surface Analysis (LESA)	Liquid Extraction		1 mm (350 μm^a)

^aThe highest lateral resolution attained for the ambient mass spectrometry imaging technique

Figure 3: Summary of various ambient ionization techniques with their respective mechanism of ionization, schematic of ion source and image resolution. Reproduced from Perez et. al.⁶⁰

1.5.1. Desorption Electrospray Ionization Mass Spectrometry (DESI-MS)

Inspired from various surface analysis techniques such as matrix assisted laser desorption ionization (MALDI) and secondary ion mass spectrometry (SIMS), Takats et al. introduced desorption electrospray ionization (DESI) in 2004 that has numerous advantages over the previous techniques (Figure 4).⁶¹ Both MALDI and SIMS require vacuum for efficient desorption and ionization while DESI being an ambient ionization technique is capable of successfully ionizing surface molecules under atmospheric pressure. Furthermore, unlike MALDI that requires intense sample preparation with matrix, DESI can directly analyze thin sample sections, sample blotted on the surface, as well as dry samples without additional sample

preparation. All these techniques have their respective advantages and disadvantages. MALDI is the most versatile method that can analyze samples ranging from small metabolites to large biological macromolecules such as proteins; however it requires the largest sample preparation time for the analysis. SIMS, on the other hand, has the highest resolution due to its smallest ion beam diameter, but it cannot operate at ambient conditions. DESI has the least sample preparation time along with the ability to manipulate samples within the experiment being conducted under atmospheric conditions, while it has moderate resolution and sample range.⁶²

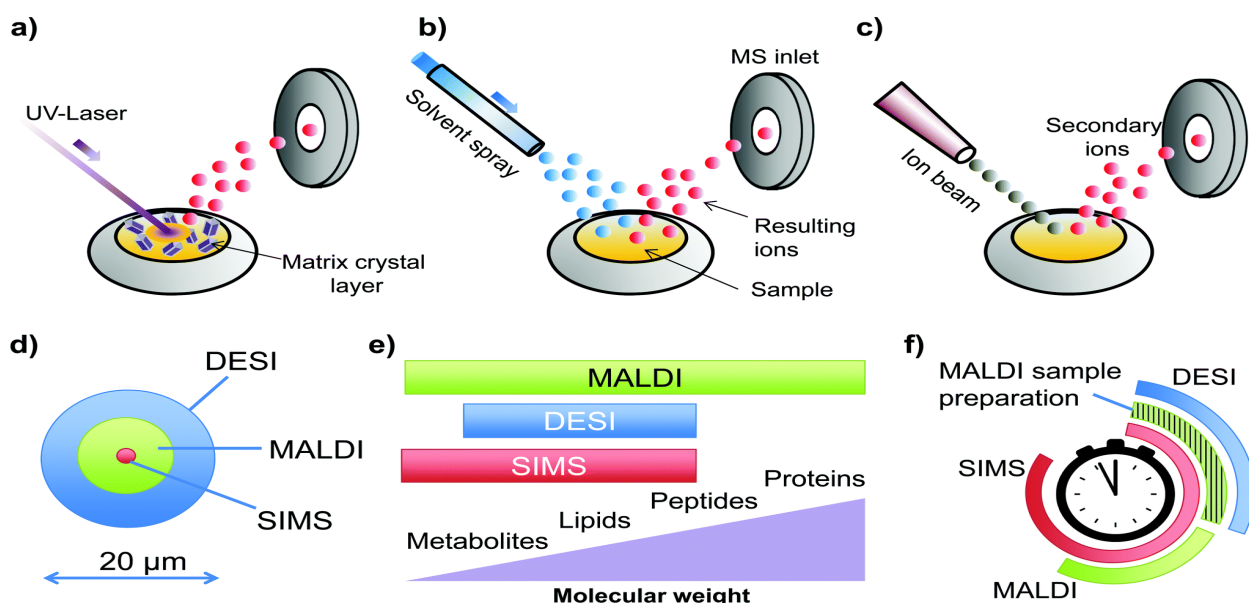


Figure 4: Conventional mass spectrometry techniques. (a) Matrix assisted laser desorption ionization (MALDI) shoots laser on sample embedded in matrix. (b) Desorption electrospray ionization (DESI) uses solvent spray to directly analyze samples (c) Secondary ion mass spectrometry (SIMS) uses pulsed ion beams to desorb molecules. Comparison of (d) spatial resolution (e) mass range capability, and (f) sample preparation requirement of MALDI, DESI and SIMS techniques. Adapted from reference.⁶²

DESI setup incorporates four major components: a spray capillary to introduce solvent at the surface, outer capillary to introduce nebulizing gas, a moving stage where the sample of interest is mounted on a specific surface, and an atmospheric pressure ion transfer line connected to the mass spectrometer to collect sample ions for MS analysis (Figure 5). DESI utilizes a solvent spray with applied voltage to initiate desorption process by the formation of primary charged solvent particles directed to the sample surface with the aid of nebulizing N₂ gas. These charged microdroplets dissolve analyte molecules upon hitting the surface and

sputters them via droplet pickup mechanism forming secondary charged particles that are directed into MS inlet.⁶³ Analyte charged particles can also be produced by a charge transfer mechanism, wherein charge from the solvent particles in gas phase gets transferred to the sample molecules on the surface with high momentum to induce sample desorption from the surface. There is also a possibility that the sample molecules first get desorbed by the impact of charged solvent particles followed by the gas phase charge transfer from solvent to analyte molecules. Combination of these ionization mechanisms occur for majority of the analytes with one of the mechanism being predominant based on the chemical nature of the analyte, composition of the solvent, and physical properties of the surface.⁶⁴

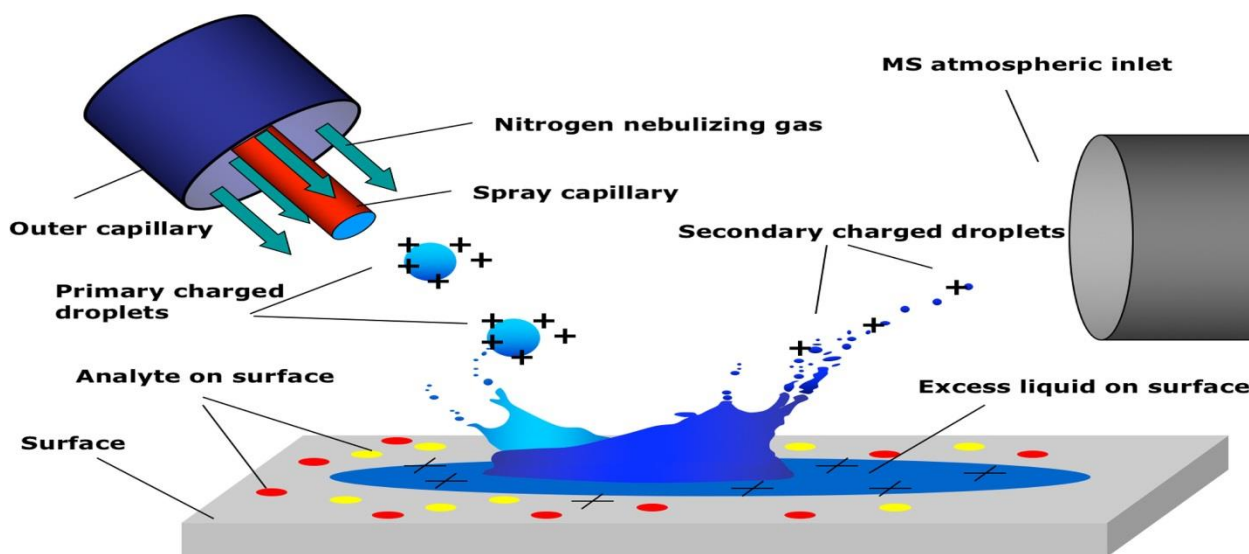


Figure 5: Schematic of sample ionization by DESI-MS. Solvent is sprayed through the inner spray capillary (red) and nebulizing gas through the outer capillary (blue). Solvent hits the surface, ionizes molecules, and creates secondary charged droplets that enter into MS inlet.⁶⁴

To ensure high ionization efficiency of DESI, optimization of certain geometrical parameters is extremely critical. These parameters include tip to surface distance, tip to inlet distance, incident angle as well as collection angle that typically works best at 2-3mm, 4-8mm, 55-60°, and 5-10° respectively for majority of the analytes (Figure 6a). The selection of an appropriate solvent is also essential since the ionization of analyte depends on the ability of solvent to dissolve analyte molecules at the sample surface. The utilization of methanol:water (1:1) and acetonitrile:water (1:1) solvent systems have been shown to efficiently ionize lipid molecules while a mixture of DMF and water have been widely employed to ionize fatty acid

moieties. The ionization efficiency of analytes can be further enhanced by the addition of weak acids such as acetic acid or formic acid into the solvent. The polarity of analyte can also be reversed by the addition of salts such as sodium acetate or formate that form adducts with the analyte molecule allowing detection of these molecules in negative ionization mode which would otherwise be detected solely in positive ionization mode.^{61,65}

1.5.2. DESI-MS Imaging

Sample images can be acquired by DESI via programmed software that provides in-depth information corresponding to relative quantitation and distribution of various metabolites within the sample (Figure 6b). The stage where the sample is mounted has the ability to move in x and y directions. The sample is segregated into a large number of pixels determined by spatial resolution, and the image is obtained by rastering along the x-direction while acquiring mass spectrum for each pixel within that row. The stage is then moved in y-direction determined by step size to the next consecutive row where the process is repeated. Once the acquisition of mass spectra for the entire sample size is completed, the data set is collated together and plotted in two-dimensional space to obtain spatial distribution of ions in the sample. A color-coding scheme can be utilized to obtain relative intensity of ions in the sample. Typically 150 μm spatial resolution is achieved by DESI; however, the resolution can be increased up to 40 μm under specific operating conditions.^{65,66}

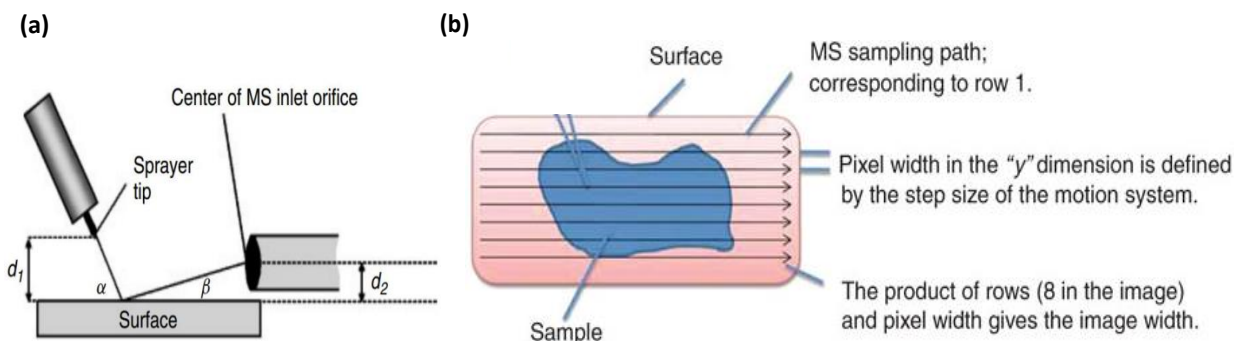


Figure 6: Schematic of (a) DESI geometric parameters with incident angle (α), collection angle (β), spray to surface distance (d_1), and MS inlet to surface distance (d_2). (b) DESI imaging that splits sample into multiple rows and acquires spectrum for each pixel within the row.^{67,68}

In recent years, DESI-MSI has been widely explored for its applications in clinical settings. It has been extensively utilized to investigate metabolite, lipid and fatty acid profiles in variety of cancers and other disease affected tissue types such as Parkinson's and Alzheimer's disease.⁶⁹ These profiles tend to alter, either in intensity or distribution, in response to disease which is targeted as a potential biomarker for disease diagnostics. Tumor tissues have been successfully segregated from normal tissues using DESI coupled with multivariate statistical analysis such as principal component analysis (PCA).⁶⁰ Recent advances in DESI have allowed accurate identification of tumor margins that are critical for efficient tumor extraction during surgical procedure. The increasing number of lipidomic research studies emphasizing the apprehension of lipid profiles of diseased state tissues indicate the significance of lipid composition for the identification of disease associated biomarkers.^{65,66}

1.6. Statistical Approach: Principal Component Analysis

Principal Component Analysis (PCA) is a multivariate statistical analysis that is most widely used to reduce dimensions of the data set. PCA analyzes observations described by numerous inter-correlated variables to extract the important information from the data table and express it as a set of linearly uncorrelated orthogonal variables called principal components. Thus, PCA transforms the data to create a new coordinate system such that the total number of variables in the data set equals total number of coordinates. The values of these new variables for the observations are called factor scores. The orthogonal transformation is defined in such a way that the first principal component has the largest possible variance, accounting for as much of the variability in the data as possible, and each succeeding component have the highest variance possible while being orthogonal to the preceding component. Thus, the first two or three components represent most of the variance in the data.^{70,71}

In this study, PCA was used to disclose the variability between three healthy and three FASD brain samples, as well as the gray and white matter of the brains. Score plots and biplots were used for data analysis as it provides simple representation of complex multidimensional

data set. A score plot represents various samples according to its score on the principal component scale such that the points closer together correspond to observations that have similar scores with less variability while the points farther apart have most variability. The region corresponding to similar scores with less variability can be highlighted by circle or ovals with different colors on the principal component axis to indicate unique clusters. The formation of distinct clusters in the score plot represents various groups of samples that have less variability within the cluster but large variability from the other sample groups.

On the other hand, biplot is the simultaneous interpretation of both rows (FASD and wildtype brain samples) and columns (phospholipid ions) that represent objects as well as vectors pointing in the direction that has the highest squared multiple correlation with the principal components.⁷² In our data set, FASD and wildtype brain samples represented points; while direction of vector corresponded to the correlation of phospholipid ions with various samples. Biplots used for multivariate statistical analysis follows an interpretation rule that the correlation of phospholipid ions with sample type is better than average if the angle between its vector and sample's vector is $<90^\circ$; while the correlation is lower than average if the angle is $>90^\circ$.⁷² Thus, the phospholipid ions that are more correlated with FASD brains point towards the FASD cluster forming an acute angle indicating positive correlation corresponding to higher abundance in FASD samples. On the other hand, phospholipid ions that point towards wildtype cluster forms an obtuse angle with FASD cluster indicating negative correlation corresponding to lower abundance in FASD samples.

1.7. Research Aims

The current study aims at monitoring the impact of alcohol on fetal brain phospholipids that plays critical role in numerous cellular pathways vital for appropriate cognitive functions. Phospholipids are the primary constituent of membrane bilayers whose disruption can alter electrophysiology of the cell. The effect of ethanol on phospholipids has been previously investigated by other techniques such as the use of fluorescent dyes and their detection by UV absorption.^{15,73,74} However, alterations in phospholipid composition and distribution in response to ethanol has not been previously explored by MS based techniques. It is

hypothesized that alcohol increases the overall level of phospholipids in the entire FASD brain as well as modulates its abundance in specific regions of the brain that leads to the adverse behavioral responses observed in these patients. In this study, the variation in phospholipid distribution was investigated by DESI-MSI as the coupling of DESI with MS imaging adds to the tremendous advantages of MS by providing an interface for sample imaging that, in addition to providing sample identification and characterization, gives insight into the distribution of molecules in different regions of the tissue sample. Furthermore, high resolution MS instrument was used to characterize phospholipid molecules as it provides sufficient mass accuracy for the calculation of exact mass and elemental composition of ion peaks for accurate identification of phospholipids in complex tissue types.⁷⁵

CHAPTER II

Experimental

2.1. Mouse Husbandry and Ethanol Treatment

This section of the study was done in collaboration with Dr. Peter Carlen at the University of Toronto. The University Health Network animal ethics committee in Toronto approved this FAS study, and all experimental procedures were performed in accordance to the recommendations of the Canadian Council on Animal Care (Protocol 2011-09-GZ). C57/BL6 male and female mice were obtained from Charles River Laboratories (Montreal, Quebec, Canada) and were subjected to ethanol consumption as described by Kaminen-Ahola et al., 2010. Briefly, 6-8 week old mice were grouped together in the same cage and were allowed to breed. Mating was confirmed by the presence of vaginal plugs in female mice whereupon male mice were removed from the cage. Drinking water was replaced with 10% (v/v) ethanol, and was voluntarily consumed by the pregnant mice from the day of mating, gestation day (GD) 0.5, to GD 7.5 corresponding to the first trimester of gestation in mouse. Control offspring were obtained from pregnant mice that were not exposed to alcohol during gestation. All experiments were conducted on male and female postnatal offspring aged 30 days that were randomly selected from control and prenatal alcohol exposure (PAE) pregnancies. Three control and three PAE litters were tested in this study.

2.2. Mouse Brain Sample Preparation and Cryosectioning

Control and PAE mice were anesthetized with an intra-peritoneal injection of pentobarbital (50-90 mg/kg body weight) and decapitated by our collaborators at University of Toronto. The brain was quickly removed and embedded in a melted solution of 2.5% carboxymethylcellulose (CMC) and 5% gelatin placed in an appropriate mold based on tissue size. The tissue orientation was adjusted appropriately and air bubbles, if present, were removed from the solution. A plastic cassette was placed on top of the mold and the embedding solution was allowed to solidify.

Coronal sections of the embedded brain were obtained using Shandon Cryotome FE and FSE from Thermo Fischer Scientific (Waltham, Massachusetts, USA). The cryostat chamber temperature, cryobar temperature and specimen temperature were modulated between -16°C and -20°C while clearance knife angle was adjusted to 2-3° in order to obtain 20µm thin tissue slices. The tissue sections were thaw mounted on microscopic glass slides and stored at -80°C until analyzed. Tissue sections were air dried for 20 minutes prior to DESI-MS analysis.

2.3. Phospholipid Extraction and Characterization using HRMS

The method of Bligh and Dyer⁷⁶ was followed for the extraction of phospholipids from brain tissue. The weight of the brain was measured using an analytical balance and the brain was transferred into glass dounce homogenizer. 3ml of a mixture of chloroform:methanol (1:2 v/v) was added per gram of tissue to homogenize the tissue. A small amount of homogenate (1ml) was removed and the remaining tissue residue was further homogenized with 1ml of chloroform per gram of tissue. The homogenates were combined and briefly centrifuged to remove tissue debris. 1ml of chloroform per gram of tissue was added into the mixture followed by the same volume of 0.9% NaCl (1ml per gram of tissue). The solution was centrifuged to induce phase separation and phospholipids were collected in the lower chloroform phase. The chloroform layer was transferred to another tube which was then dried under a nitrogen stream and re-suspended in methanol for HRMS analysis.

High mass accuracy analysis and tandem MS of phospholipid extract was obtained using LTQ Orbitrap Elite mass spectrometer (Thermo Fischer Scientific, Bremen, Germany). Full scan mass spectra were recorded in the mass range of m/z 500-1000 at sample flow rate of 5µL/min. The spray voltage was set to 4kV and capillary temperature to 250°C. Tandem MS were acquired at the normalized collision energy of 20-25% with mass resolving power of 100,000 FWHM and isolation window of m/z 0.5-1.

2.4. DESI-MS and DESI-MS Imaging

DESI-MS was performed using a laboratory built ionization source, similar to the commercial source from Prosolia, Inc., coupled to a linear ion trap mass spectrometer (LTQ) operated by XCalibur 2.0 software (Thermo Fischer Scientific). Glass slides containing brain sections were mounted on the moving stage capable of moving in xyz direction and were analyzed in both positive and negative ionization modes over the mass range of m/z 500 to 1000. Pure methanol was used as the spray solvent and delivered at a flow rate of 5 $\mu\text{L}/\text{min}$. The sprayer to surface distance was set at 2 mm, sprayer to MS inlet distance at 5 mm, and incident angle at 62° . The typical source parameters used were automatic gain control (AGC) off, 200 ms maximum injection time with 3 microscans, 250° capillary temperature, and 100 PSI nitrogen gas pressure.

For DESI-MS imaging, brain tissue size was measured and sample scan rate was calculated based on the desired image resolution of 150 μm , flow rate of 5 $\mu\text{L}/\text{min}$ and scan time of 0.82 s. The sample was segregated into multiple rows defined by resolution and the tissue was raster scanned at a constant velocity of 183 $\mu\text{m}/\text{s}$. Mass spectra were obtained for all the rows and Xcalibur 2.0 mass spectral data set was converted into BioMap compatible format using ImageCreator version 3.0 that allowed the processing of spectral data to generate 2D spatially resolved ion images.

Statistical analysis, specifically principal component analysis (PCA), was performed on the entire brains as well as gray and white matter of FASD and healthy brains using metaboanalyst software.⁷⁷ Region of interest (ROI) was selected in Biomap that provides an average mass spectrum corresponding to the designated area. ROI dataset was further processed using mMass software in which data was filtered using 5-8% and 25% relative intensity threshold and baseline correction was also implemented. Data was normalized to the base peak referring to the most intense peak in mass spectrum.

CHAPTER III

Results and Discussion

3.1. Phospholipid Identification by DESI-MS

FASD and control mouse brains were cryosectioned into 20 μ m thin slices, thaw mounted on glass slides and directly analyzed using DESI-MS. The spectrum obtained by DESI-MS shows multiple molecular ion species in positive ionization mode ranging from m/z 756.5 to m/z 872.3 (Figure 5 a, b); while negative ionization mode results in the ion peaks ranging from m/z 788.5 to m/z 917.4 (Figure 5 c, d).

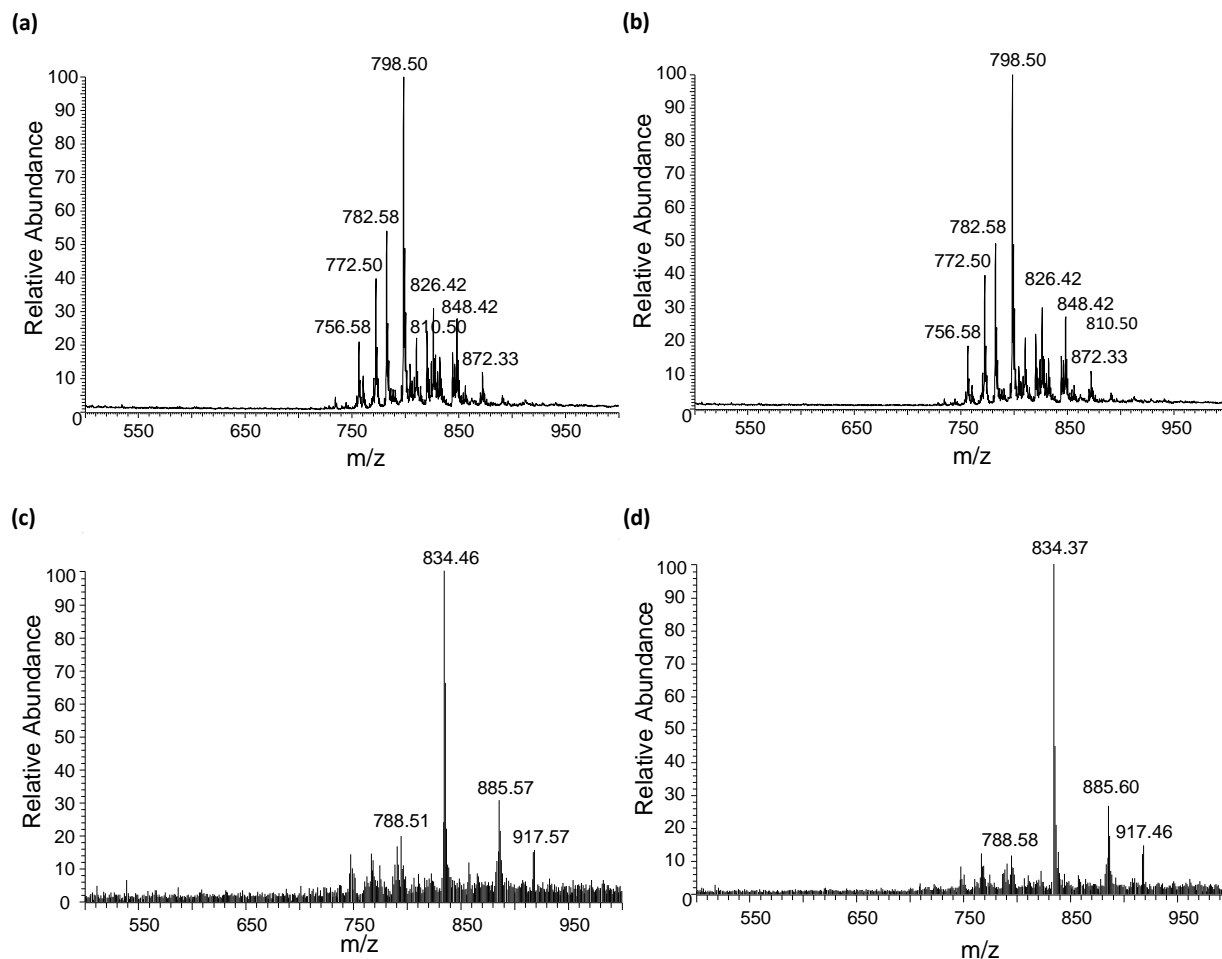


Figure 7: Full Scan DESI-MS spectra of (a) control mouse brain tissue in positive ion mode, (b) FASD mouse brain tissue in positive ion mode, (c) control mouse brain tissue in negative ion mode, (d) FASD mouse brain tissue in negative ion mode. Methanol was used as a spray solvent at 5 μ L/min flow rate.

Identical phospholipid ions were observed in control and FASD brain sections in both positive and negative ionization modes with the ion at m/z 798 being the most abundant ion detected in positive ionization mode and the ion at m/z 834 being the predominant ion in negative ionization mode. Although FASD brain illustrated similar phospholipids as that of the healthy brain, the relative abundance of these phospholipids varied significantly (Figure 7). Furthermore, the relative abundance of these phospholipids was also observed to alter with respect to the position within the brain section being analyzed by DESI. Thus, multiple spectra for the entire brain section were collected and the information was integrated prior to the multivariate statistical analysis. The phospholipid intensities in large number of mass spectra collected throughout the section were mapped together to obtain 2D ion images depicting localization of these phospholipids within the brain section.

The impact of alcohol on gray and white matter of FASD brain samples was investigated in both positive and negative ionization mode. These two regions of interest display unique spectral features with distinct phospholipid distribution in healthy brain which was compared with its distribution in FASD brain to explore the variations caused by alcohol. In positive ionization mode, both FASD and wildtype brain samples showed higher signal intensity for ion at m/z 782 in gray matter of the brain. In contrast, the most predominant ion detected in white matter of the brain corresponded to the ion at m/z 798 in positive ion mode (Figure 8).

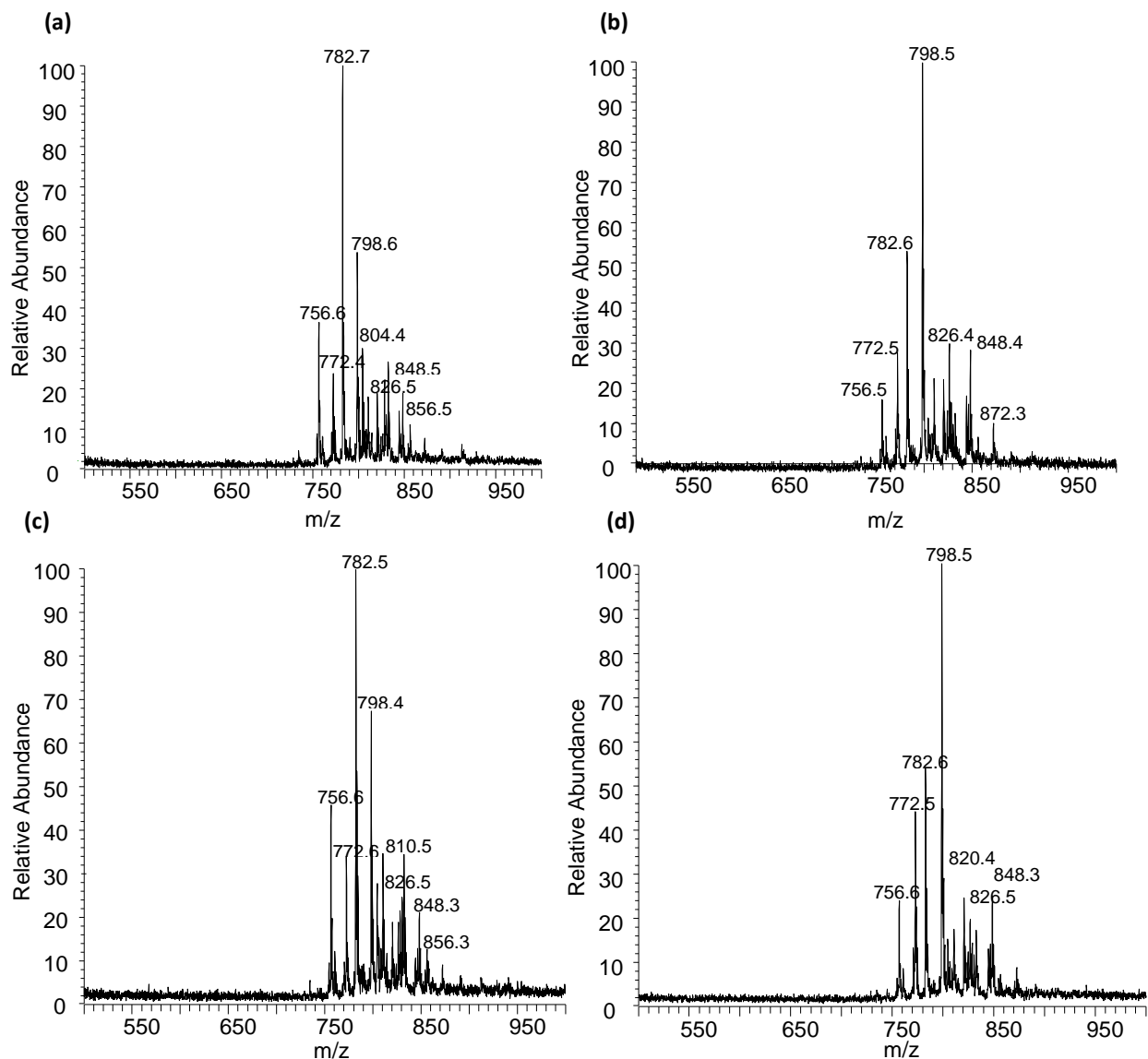


Figure 8: Full Scan DESI-MS spectra in positive ionization mode. (a) MS spectrum corresponding to gray matter of healthy brain. (b) MS spectrum corresponding to white matter of healthy brain. (c) MS spectrum acquired in gray matter of FASD brain. (d) MS spectrum acquired in white matter of FASD brain. Methanol was used as a spray solvent at 5 μ L/min flow rate.

Negative ionization mode also illustrated similar phospholipid ions in respective regions of interest in FASD and wildtype brains. The ion at m/z 834 was detected to be the most abundant ion in gray matter of the brain; while, the signal intensity of ion at m/z 788 was most abundant in white matter of the brain (Figure 9). The signal intensity of other phospholipids with respect to the base peak varied remarkably among FASD and healthy brains. The extent of variation in phospholipid intensity as well as its distribution could not be directly elucidated from DESI-MS spectrum. As a result, principal component analysis (PCA), a powerful statistical

tool, was performed on the entire brain as well as gray and white matter of FASD and healthy brains to determine the magnitude of variation.

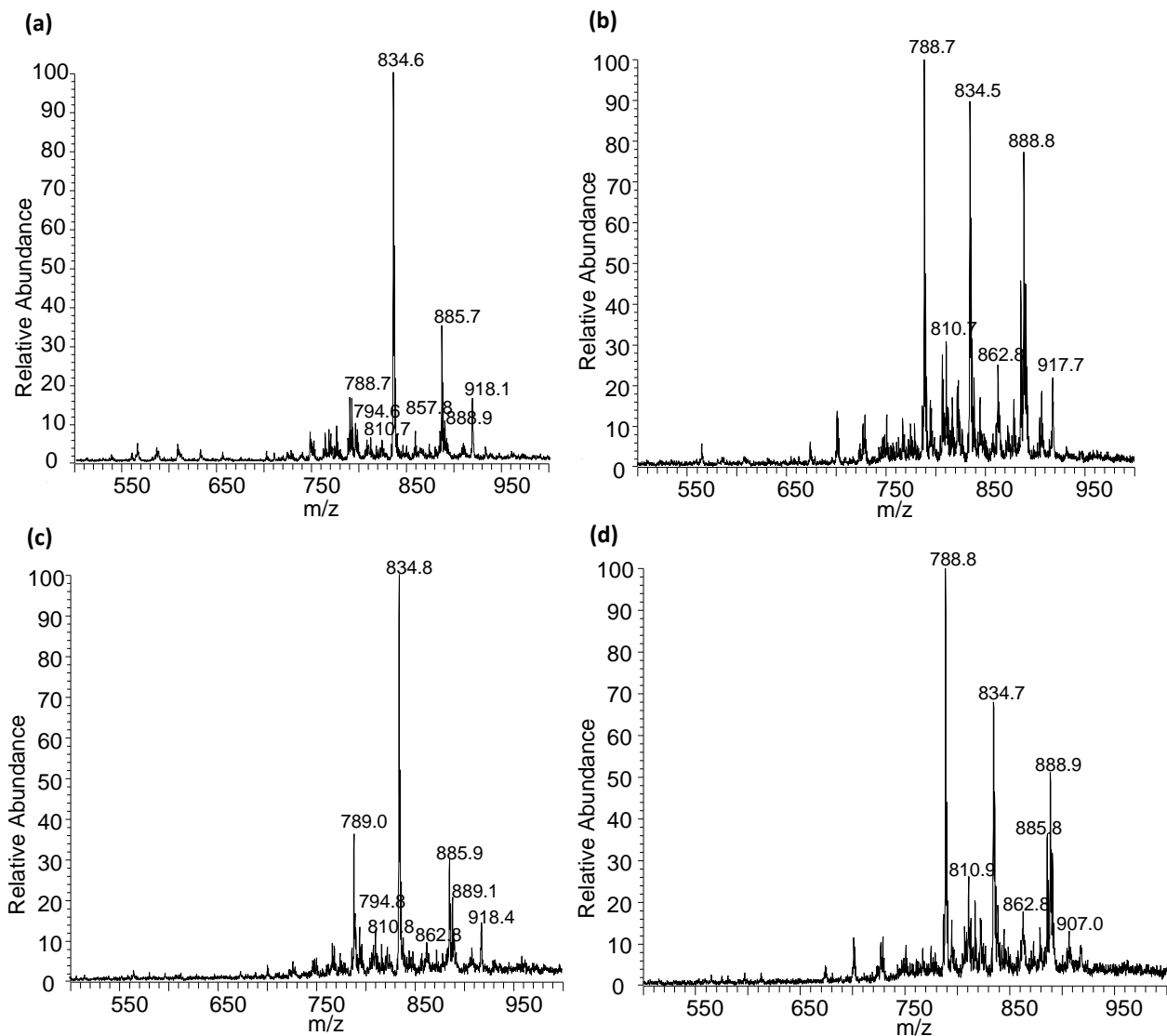


Figure 9: Full Scan DESI-MS spectra in negative ionization mode. (a) MS spectrum acquired in gray matter of healthy brain. (b) MS spectrum acquired in white matter of healthy brain. (c) MS spectrum corresponding to gray matter of FASD brain. (d) MS spectrum corresponding to white matter of FASD brain. Methanol was used as a spray solvent at 5 μ L/min flow rate.

3.2. Phospholipid Characterization by HRMS

Prior to the imaging and statistical analysis of phospholipid ion molecules, the ions were characterized using electrospray ionization (ESI) coupled to high resolution mass spectrometry. Lipid extract analyzed by ESI-HRMS resulted in the detection of additional molecules which were not previously observed by DESI (Figure 10 a,b). Furthermore, the relative abundance of phospholipids observed in DESI and ESI spectra varied significantly. Such spectral differences originated from the unique ionization processes associated with the techniques. DESI, being surface analysis technique, ionized molecules primarily at the surface of the sample while lipid extract obtained from the whole brain tissue comprised of all the lipids existing within the tissue which was detected by ESI.

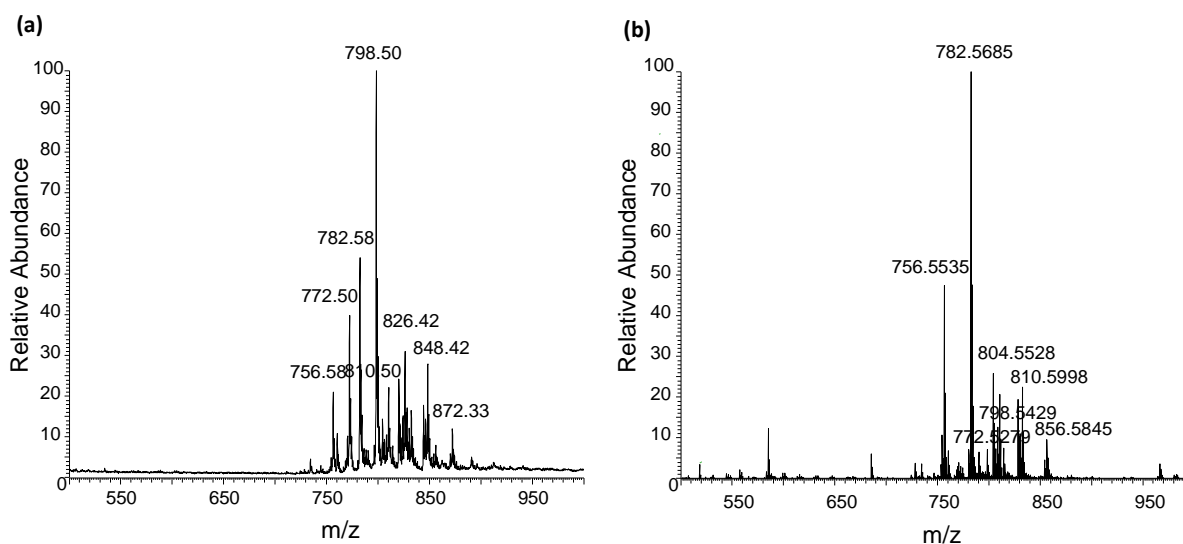


Figure 10: Full Scan MS spectra of (a) mouse brain tissue section acquired by DESI-MS and (b) mouse brain lipid extract acquired by ESI-HRMS.

The molecular ion peaks observed in DESI were selected for further fragmentation in ESI. The fragmentation of ion at m/z 756.5 resulted in the loss of 59 Da corresponding to the characteristic loss of phosphatidylcholine head group, $[N(CH_3)_3]$, at m/z 697.5 (Figure 11). Neutral loss of 16 carbon alkyl chain $[C_{15}H_{31}COOH]$ at m/z 500.3 and sodium ion at m/z 551.5 was also detected; thereby characterizing the molecule as sodium adduct of phosphatidylcholine $[PC(16:0/16:0) + Na]^+$ with mass error of 1.3 ppm.

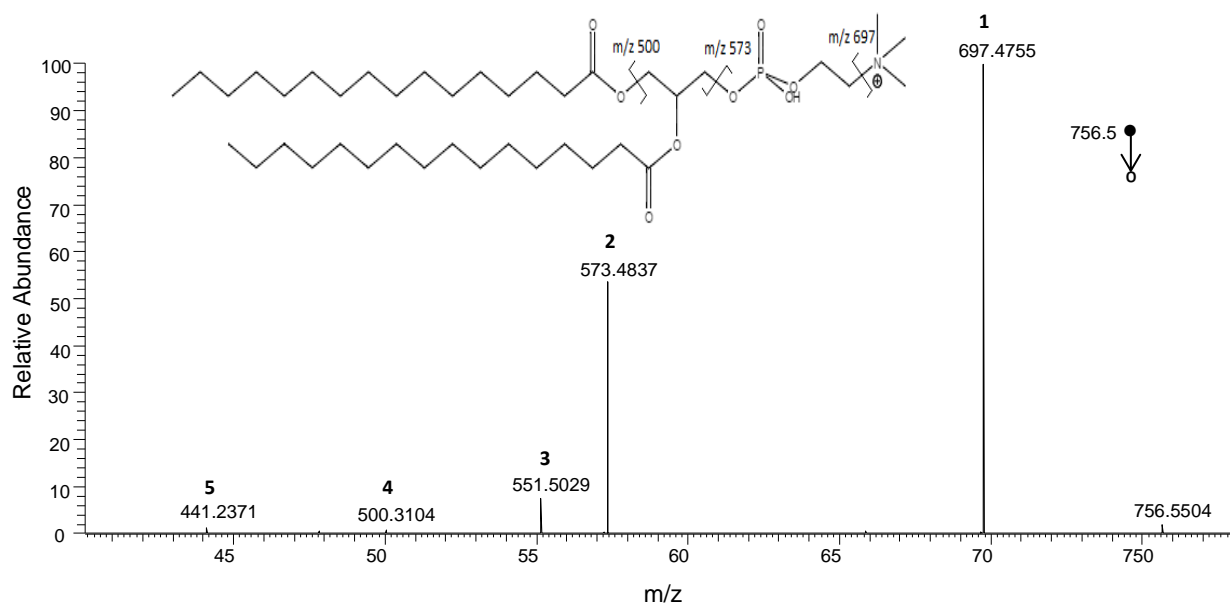


Figure 11: ESI MS/MS spectra of phosphatidylcholine $[\text{PC}(16:0/16:0) + \text{Na}]^+$ at m/z 756.5504 with its fragment ions (1) $[\text{PC}(16:0/16:0) + \text{Na} - \text{N}(\text{CH}_3)_3]^+$ at m/z 697.4755; (2) $[\text{PC}(16:0/16:0) + \text{Na} - \text{C}_5\text{H}_{14}\text{NPO}_4]^+$ at m/z 573.4837; (3) $[\text{PC}(16:0/16:0) - \text{Na} - \text{C}_5\text{H}_{14}\text{NPO}_4]^+$ at m/z 551.5029; (4) $[\text{PC}(16:0/16:0) + \text{Na} - \text{C}_{15}\text{H}_{31}\text{COOH}]^+$ at m/z 500.3104; (5) $[\text{PC}(16:0/16:0) + \text{Na} - \text{C}_{15}\text{H}_{31}\text{COOH} - \text{N}(\text{CH}_3)_3]^+$ at m/z 441.2371.

Table 2: Phospholipid ion characterization in positive ionization mode using ESI-HRMS.

Characteristic Ions (m/z)	Ion Identification	ESI Fragment Ions (m/z)
756.5502	$[\text{PC}(16:0/16:0)+\text{Na}]^+$	697, 573, 551, 500, 441
772.5214	$[\text{PC}(16:0/16:0)+\text{K}]^+$	713, 589, 567, 551
772.5214	$[\text{PE}(\text{P}-16:0/22:6)+\text{Na}]^+$	729, 631, 609, 488, 463, 305
782.5624	$[\text{PC}(16:0/18:1)+\text{Na}]^+$	723, 599, 577, 467, 441
798.5390	$[\text{PC}(16:0/18:1)+\text{K}]^+$	739, 615, 441
798.5390	$[\text{PE}(\text{P}-18:0/22:6)+\text{Na}]^+$	755, 657, 487
826.5725	$[\text{PC}(18:0/18:1)+\text{K}]^+$	767, 643, 605

The molecular ion peak at m/z 772.5 was also subjected to fragmentation and was identified as a mixture of phosphatidylcholine $[\text{PC}(16:0/16:0)+\text{K}]^+$ and phosphatidylethanolamine $[\text{PE}(\text{P}-16:0/22:6)+\text{Na}]^+$ species (Figure 12). Neutral loss of 59 Da specific to PC phosphate head group was seen at m/z 713.4 identifying it as $[\text{PC}(16:0/16:0)+\text{K}]^+$

with a mass error of 2.1 ppm (Figure 12b). On the other hand, phosphatidylethanolamine fragmentation lead to the characteristic loss of 43 Da also associated with its head group followed by the loss of 16 and 22 carbon alkyl chains at m/z 488.2 and m/z 305.3 respectively (Figure 12c). Neutral loss of sodium was also detected and the phospholipid molecule was identified as $[\text{PE}(\text{P-16:0}/22:6)+\text{Na}]^+$ with a mass error of 4.5 ppm. The identification of all other phospholipids is summarized in Table 2. Similar characterization was also performed in negative ionization mode using ESI coupled to LTQ-XL mass spectrometer as shown in Table 3. Among the five major ions identified by DESI, three of the ions corresponded to phosphatidylserine linked with unique fatty acid chains; while, the other two ions were characterized as phosphatidylinositol and sulfatide.

Table 3: Phospholipid ion characterization in negative ionization mode using ESI coupled to LTQ-XL mass spectrometer.

Characteristic Ions (m/z)	Ion Identification
788	$[\text{PS}(18:0/18:1)]^-$
810	$[\text{PS}(18:0/20:0)]^-$
834	$[\text{PS}(18:0/22:6)]^-$
885	$[\text{PI}(18:0/20:4)]^-$
888	$[\text{ST}(24:1)]^-$

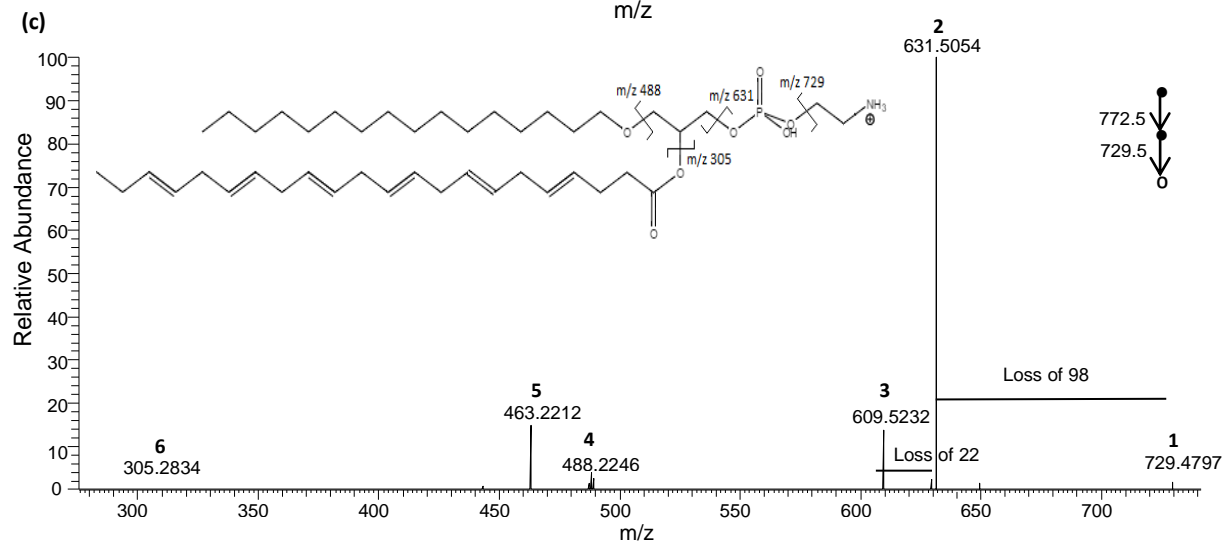
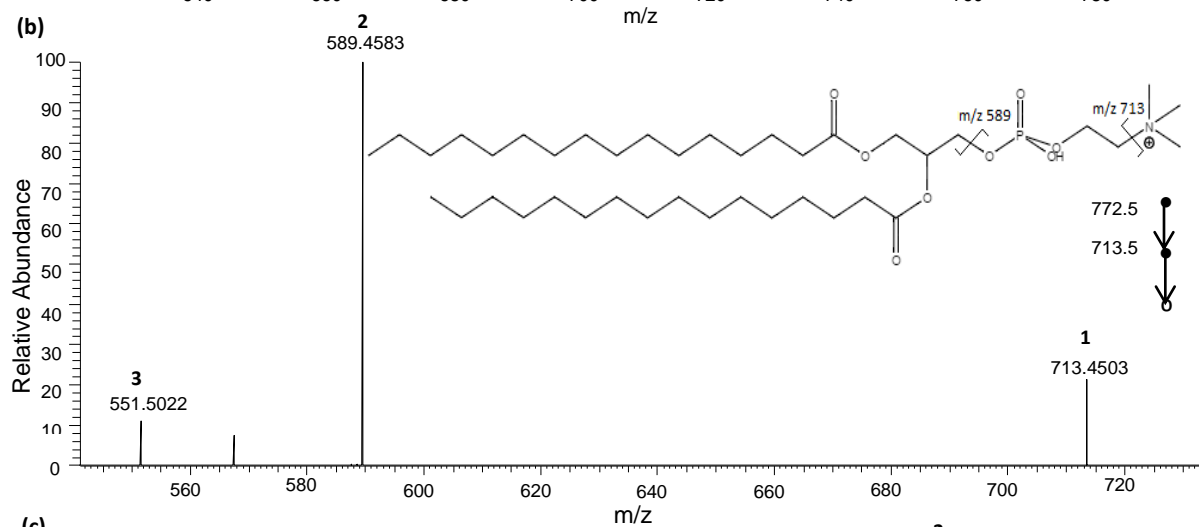
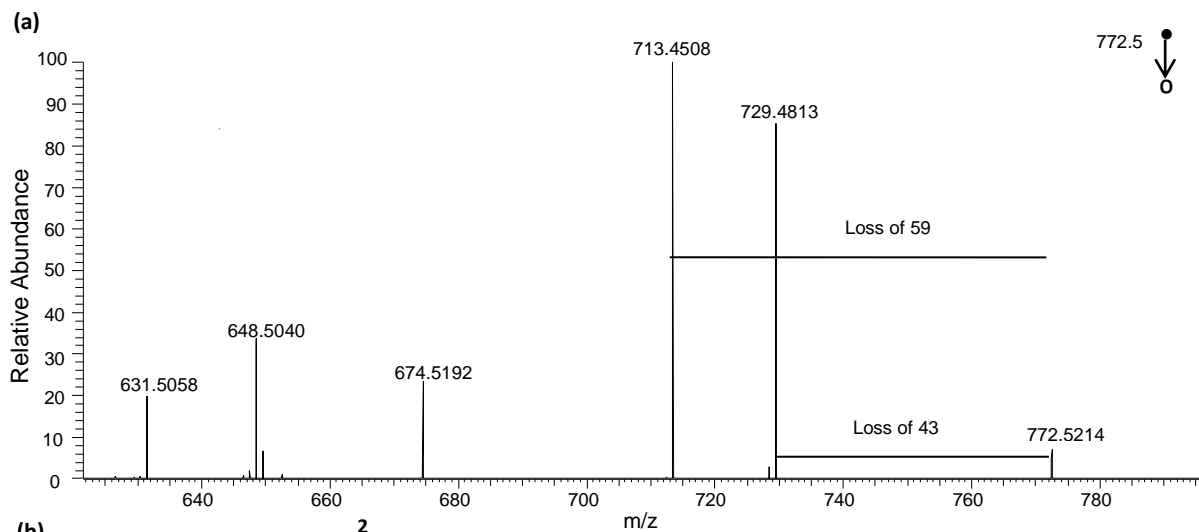


Figure 12: ESI-HRMS spectra of control brain in positive ionization mode. (a) MS/MS Scan of molecule at m/z 772.5. (b) MS3 of ion (1) $[\text{PC}(16:0/16:0)+\text{K}-\text{N}(\text{CH}_3)_3]^+$ at m/z 713.5 with fragment ions (2) $[\text{PC}(16:0/16:0)+\text{K}-\text{C}_5\text{H}_{14}\text{NPO}_4]^+$ at m/z 589, and (3) $[\text{PC}(16:0/16:0)-\text{N}(\text{CH}_3)_3]^+$ at m/z 551. (c) MS3 of ion (1) $[\text{PE}(\text{P}-16:0/22:6)+\text{Na}-\text{C}_2\text{H}_5\text{N}]^+$ at m/z 729 with fragment ions (2) $[\text{PE}(\text{P}-16:0/22:6)+\text{Na}-\text{C}_2\text{H}_8\text{NPO}_4]^+$ at m/z 631, (3) $[\text{PE}(\text{P}-16:0/22:6)-\text{Na}-\text{C}_2\text{H}_8\text{NPO}_4]^+$ at m/z 609, (4) $[\text{PE}(\text{P}-16:0/22:6)+\text{Na}-\text{C}_{15}\text{H}_{32}\text{CHO}-\text{C}_2\text{H}_5\text{N}]^+$ at m/z 488, (5) $[\text{PE}(\text{P}-16:0/22:6)-\text{Na}-\text{C}_{15}\text{H}_{32}\text{CHO}-\text{C}_2\text{H}_5\text{N}]^+$ at m/z 463, and (6) $[\text{PE}(\text{P}-16:0/22:6)+\text{Na}-\text{C}_{21}\text{H}_{29}\text{COOH}-\text{C}_2\text{H}_8\text{NPO}_4]^+$ at m/z 305.

3.3. DESI-MS Imaging

DESI-MS images of FASD and control brain sections were acquired in both positive and negative ionization modes. The images were normalized to the base peak corresponding to the ion at m/z 798 in positive ion mode and the ion at m/z 834 in negative ion mode to account for signal intensity variations that were not associated with the biological tissue and solely arise from image acquisition. The distribution of phospholipids in 30 day old wildtype and FASD mice brains in positive ionization mode is illustrated in Figure 13 (a,b). The image at m/z 756 corresponding to sodium adduct of PC (16:0/16:0) was localized in the cortical region; while a mixture of potassium adduct of PC (16:0/16:0) and sodium adduct of PE (P-16:0/22:6) collectively ionized at m/z 772 was primarily dispersed in cortical region, hippocampus and thalamic regions corresponding to the gray matter of FASD and control brains. On the other hand, homogeneous distribution was encountered throughout the brain except lateral ventricles for sodium adduct of PC (16:0/18:1) at m/z 782 and the amalgam of potassium adduct of PC (16:0/18:1) and sodium adduct of PE (P-18:0/22:6) at m/z 798. The ion image at m/z 826, identified as PC (18:0/18:1), illustrated PC distribution in corpus callosum and fimbria of hippocampus associated with the white matter of the brain. Among all the phospholipids identified by DESI, PC (18:0/18:1) exhibited lower signal intensity in FASD brain suggesting reduced PC levels in the white matter. On the contrary, all other phospholipids had significantly greater signal intensity in the FASD brain as compared to the control indicating clear modulation of phospholipid concentration in response to the alcohol consumption.

Significant variation in relative phospholipid concentration of wildtype and FASD brains was also observed in DESI-MS images acquired in negative ionization mode (Figure 13 c,d). PS

(18:0/18:1) at m/z 789, PS (18:0/20:0) at m/z 811 and ST (24:1) at m/z 889 were predominantly dispersed in corpus callosum and fimbria of hippocampus corresponding to the white matter of the brain. While PS (18:0/22:6) and PI (18:0/20:4) at m/z 835 and m/z 886 respectively were distributed throughout FASD and control brains. None of the phospholipids were solely localized in the gray matter of the brain that would allow direct comparative analysis between gray and white matter through DESI-MS images. Signal intensity of all the phospholipids was greater in FASD brains as compared to the control suggesting higher abundance of PS and ST species in the brain.

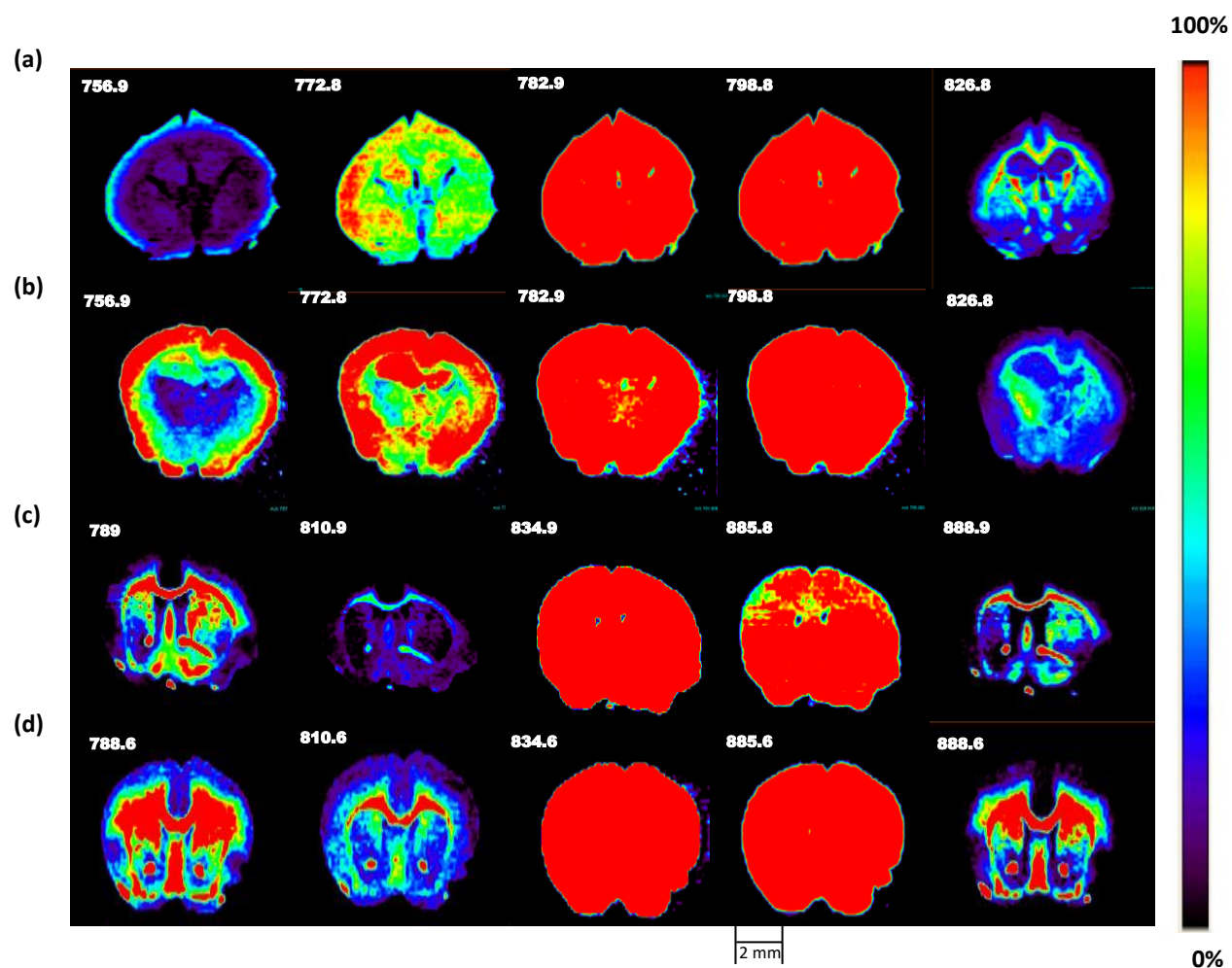


Figure 13: DESI-MS images depicting phospholipid distribution in (a) control and (b) FASD brain sections of 30 day old mice acquired in positive ionization mode and (c) control and (d) FASD brain sections of 30 day old mice acquired in negative ionization mode. Images were collected at a resolution of 150 μm .

3.3.1. Principal Component Analysis in Positive Ionization Mode

Principal Component Analysis (PCA) was executed on lipid profiles extracted through various regions of interest (ROI) corresponding to whole brain, gray matter and white matter in both positive and negative ionization mode. Three wildtype and three FASD brains of same age were cryosectioned and imaged independently for PCA analysis using Metaboanalyst software (<https://www.metaboanalyst.ca>; updated and maintained by Xia lab at McGill University). The ions for analysis were baseline corrected and further processed using mMass software (<http://www.mmass.org>) using two different selection criteria prior to PCA analysis. Both the criteria were set at signal to noise ratio (S/N) of 1; while they varied in relative abundance threshold ranging from 5% to 8% for the first criterion and 25% for the second criterion. Metaboanalyst was used to auto-scale the data set by mean centering the data set followed by dividing the data set by standard deviation of each variable.⁷⁸ The data set was also normalized to the base peak that was unique in regions of interest associated with whole brain, gray matter and white matter of the brain.

The entire brain PCA analysis in positive ion mode were assessed by both low and high relative abundance threshold criteria employed in mMass. The lower threshold data processing resulted in approximately 14 to 17 common ions in 6 samples that included 5 major ions detected in DESI-MS images along with other phospholipids prevailing in lower abundance. The PCA analysis computed subsequent to data set normalization by signal intensity of base peak (the ion at m/z 799) could not separate FASD and wildtype samples in score plot due to the contribution of low intensity phospholipids that did not vary significantly among FASD and control brains (Figure 14). On the other hand, 25% intensity threshold only resulted in 5 major ions of interest and its associated score plot obtained through PCA analysis illustrated adequate separation among FASD and control brains (Figure 15a). Consequently, 25% threshold was used for further data analysis.

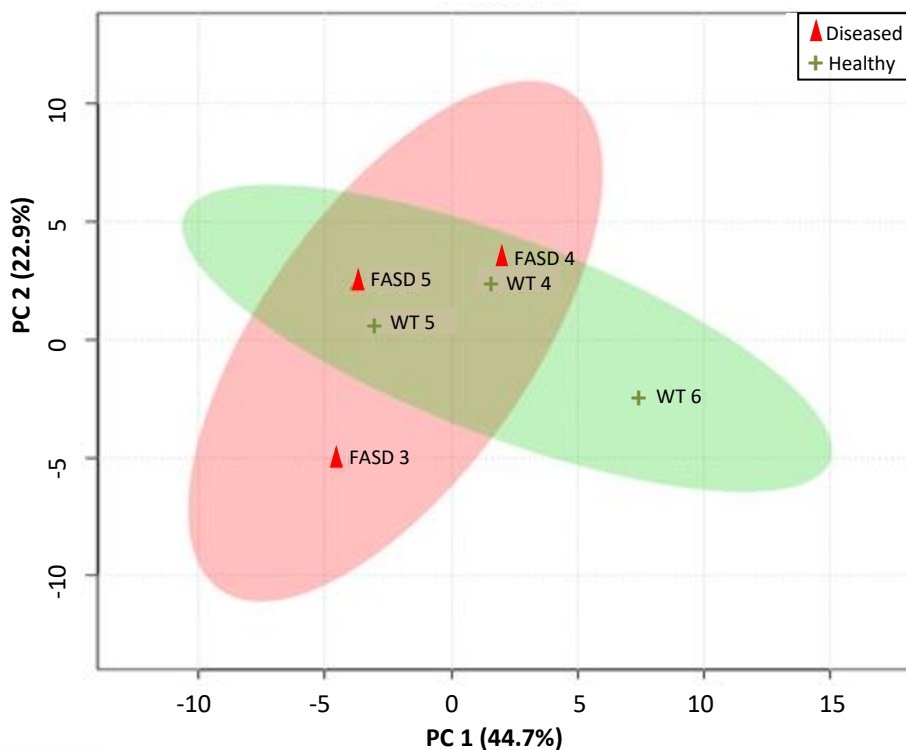


Figure 14: Principal Component Analysis score plot of FASD samples in positive ionization mode. Six mice samples including three wildtype (highlighted in green) and three FASD brain tissues (highlighted in pink) were subjected to PCA analysis. Principal component 1 and 2 (PC 1 and PC 2) corresponding to 44.7% and 22.9% variability in the data set were plotted on x and y axis respectively. The dataset was normalized to the base peak at m/z 798. PCA analysis was executed on 16 ions corresponding to entire brain ROI using 5% to 8% relative intensity threshold selection criteria.

Biplot obtained from the PCA analysis of whole FASD and wildtype brain showed that the vector of ions corresponding to m/z 826 and m/z 782 formed acute angle with wildtype cluster while obtuse angle with FASD cluster (Figure 15b). Since the interpretation rule of biplot suggests that the phospholipid ions are more correlated if their vectors form acute angle with the sample score, it indicates that these phospholipid ions are more abundant in the wildtype brain. Similarly, the vector of ions at m/z 756 and m/z 772 formed acute angle with FASD cluster while obtuse angle with wildtype cluster indicating that these phospholipid ions have higher than average correlation with FASD as opposed to wildtype. Thus, the abundance of these phospholipids was demonstrated to be higher in FASD brain in comparison to the control.

These results correlate well with DESI-MS images that depict higher signal intensity of ions at m/z 756 and 772 in FASD brain illustrated by red color.

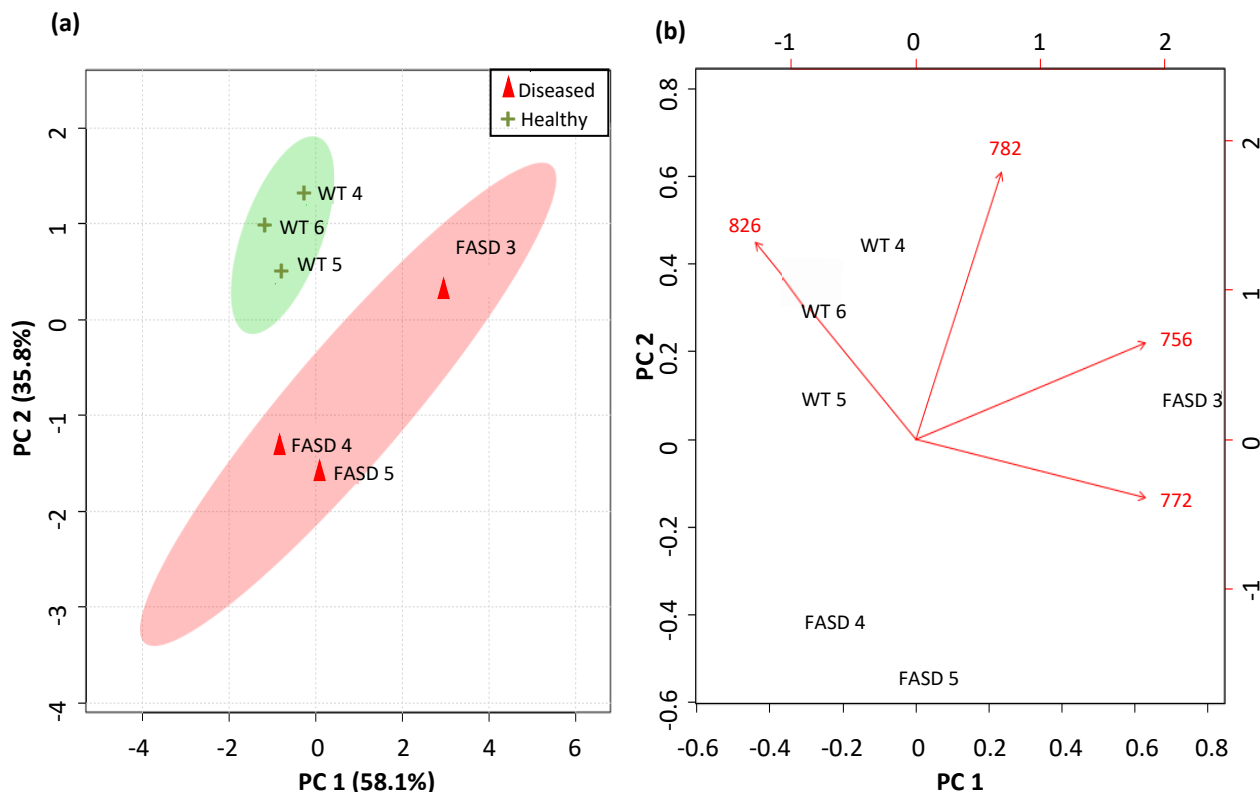


Figure 15: Principal Component Analysis of FASD samples in positive ionization mode. PCA analysis was computed using entire brain area selected as the region of interest. Six mice samples comprising three wildtype (green) and three FASD (pink) brain tissues were subjected to PCA analysis. Principal component 1 and 2 (PC1 and PC2) corresponding to 58.1% and 35.8% variability in the data set were plotted on x-axis and y-axis respectively. The dataset was normalized to the base peak at m/z 798. (a) PCA score plot with wildtype (WT) and FASD objects representing average mass spectrum obtained from whole brain ROI of each sample. (b) PCA biplot indicates contribution of various phospholipid ions in the separation of FASD and wildtype tissue samples. The ions at m/z 782 and m/z 826 formed acute angle with wildtype cluster and were consequently more abundant in wildtype brains. While, the ions at m/z 756 and m/z 772 formed acute angle with the FASD cluster and were consequently more abundant in FASD brains.

PCA analysis was also conducted on gray and white matter to explore the effect of alcohol on the distribution of phospholipids within the brain. PCA analysis could clearly distinguish gray and white matter in both wildtype and FASD tissues; while the distribution of phosphatidylcholine species was unique in both the brains (Figure 16, 17).

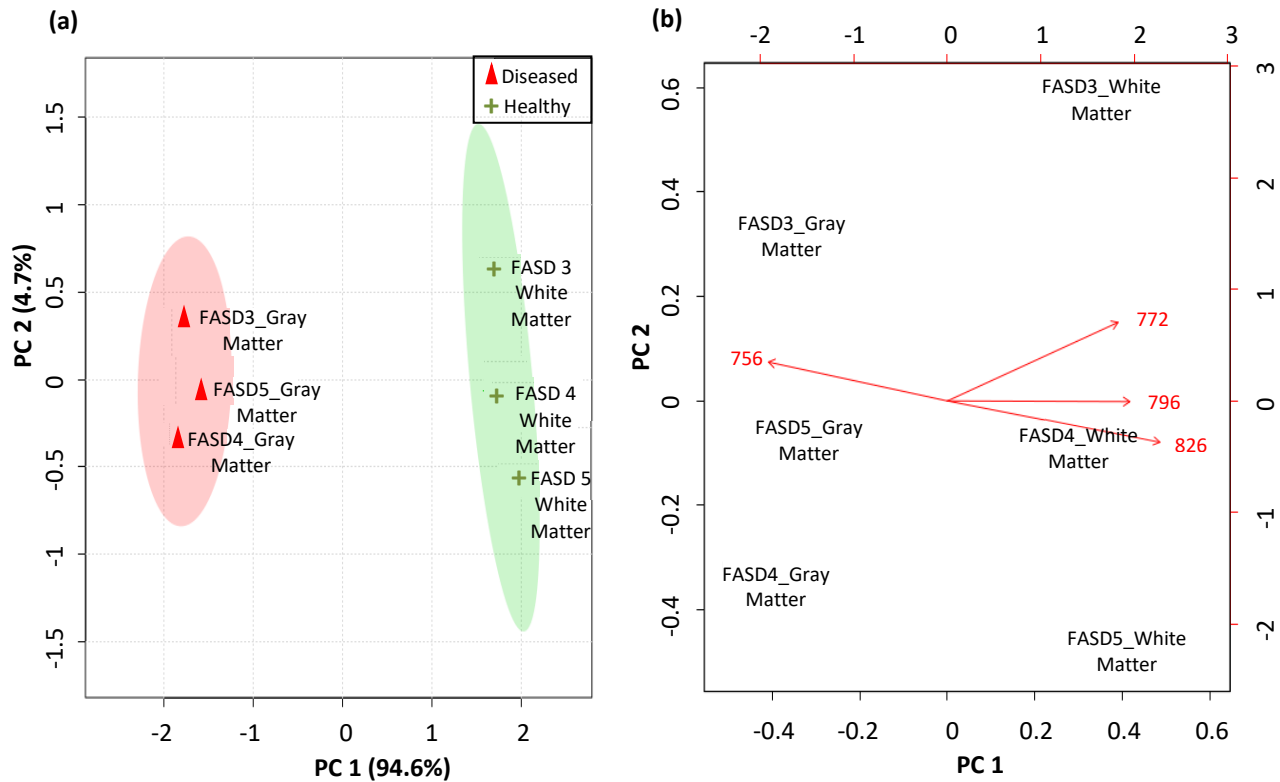


Figure 16: Principal Component Analysis of FASD samples in positive ionization mode. PCA analysis was conducted on gray (pink) and white matter (green) ROI. Principal component 1 and 2 (PC1 and PC2) corresponding to 94.6% and 4.7% variability in the data set were plotted on x-axis and y-axis respectively. The dataset was normalized to the base peak at m/z 782. (a) PCA score plot include objects depicting average mass spectrum obtained from respective ROI of each sample. (b) PCA biplot indicates contribution of various phospholipid ions in the separation of gray and white matter of FASD tissue samples. The ion at m/z 756 formed acute angle with the cluster of gray matter and was consequently more abundant in the gray matter as opposed to the white matter of FASD brains. All other ions formed acute angle with the cluster of white matter and were consequently more abundant in the white matter of FASD brains.

Sodium adduct of PC (16:0/16:0) at m/z 756 was more abundant in the gray matter of both FASD (Figure 16b) and healthy brains (Figure 17b) in comparison to their respective white matters indicating that the distribution of this phospholipid was not impacted by alcohol. However, PCA analysis of gray matter in both FASD and wildtype brains indicated higher abundance of ion at m/z 756 in FASD brains as opposed to wildtype (Figure 18b). A similar trend was observed in the PCA analysis of white matter in FASD and wildtype brains (Figure

19b) suggesting that PC(16:0/16:0) is more abundant in FASD brain in comparison to the control.

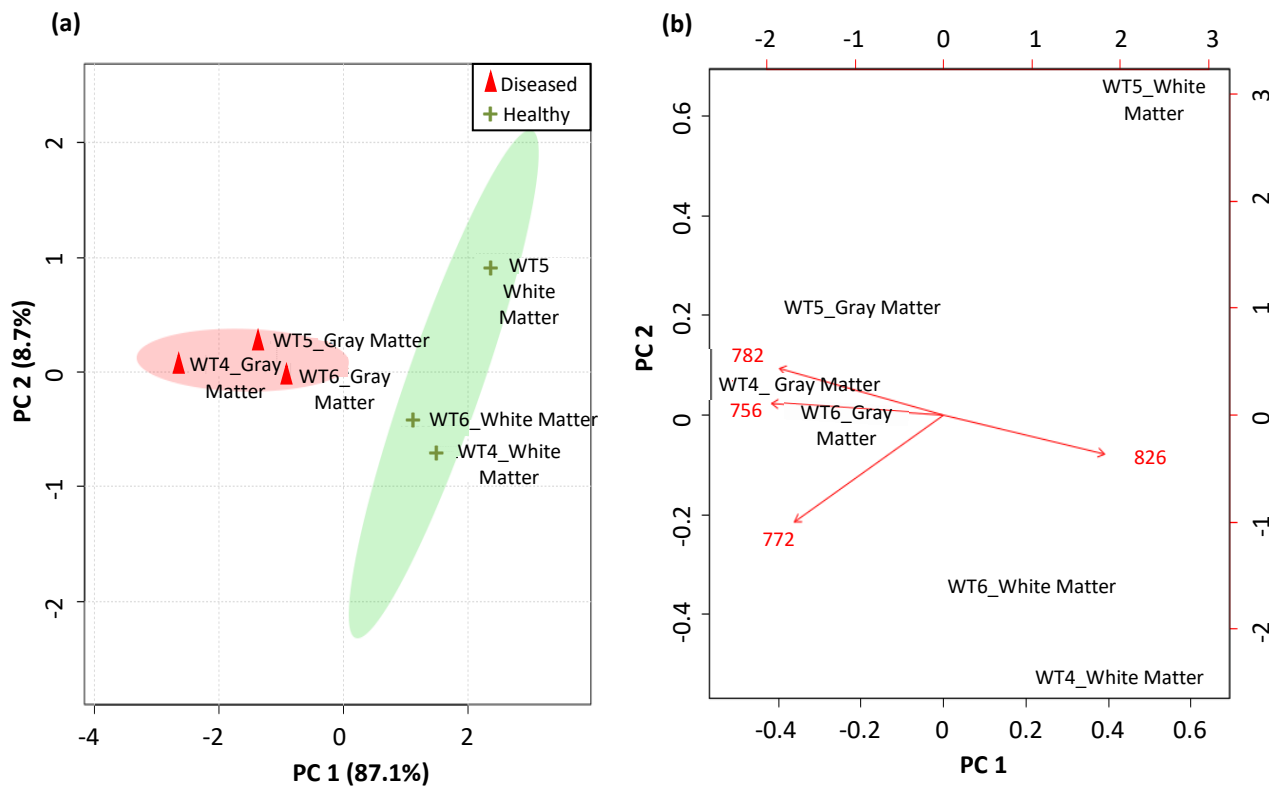


Figure 17: Principal Component Analysis of wildtype samples in positive ionization mode. PCA analysis was performed on region of interest corresponding to gray (pink) and white (green) matter of healthy brain. Principal component 1 and 2 (PC1 and PC2) corresponding to 87.1% and 8.7% variability in the data set were plotted on x-axis and y-axis respectively. The dataset was normalized to the base peak at m/z 798. (a) PCA score plot include points representing average mass spectrum of each sample obtained from its respective ROI. (b) PCA biplot shows contribution of various phospholipid ions in the separation of gray and white matter of healthy mouse brain samples. The ion at m/z 826 formed acute angle with the cluster of white matter and was consequently more abundant in the white matter as opposed to the gray matter of healthy brains. All other ions formed acute angle with the cluster of gray matter and were consequently more abundant in the gray matter of healthy brains.

The ion at m/z 772 corresponding to potassium adduct of PC(16:0/16:0) and sodium adduct of PE(P-16:0/22:6) was more abundant in the entire FASD brain in comparison to healthy brain (Figure 15b). Distribution of these phospholipids varied among both the brains such that the signal intensity of these phospholipids was greater in white matter of FASD brain in comparison to its gray matter (Figure 16b); while, in the case of healthy brain, their signal

intensity was greater in the gray matter as opposed to the white matter (Figure 17b). These results were further validated by PCA analysis of FASD and wildtype gray matter that illustrated higher abundance in the healthy brain as opposed to FASD (Figure 18b). In contrast, PCA analysis of FASD and control white matter indicated higher abundance in the FASD brain (Figure 19b). These results indicate that alcohol not only increases the overall relative abundance of phosphatidylcholine and phosphatidylethanolamine, but also enhances its distribution in white matter of the brain.

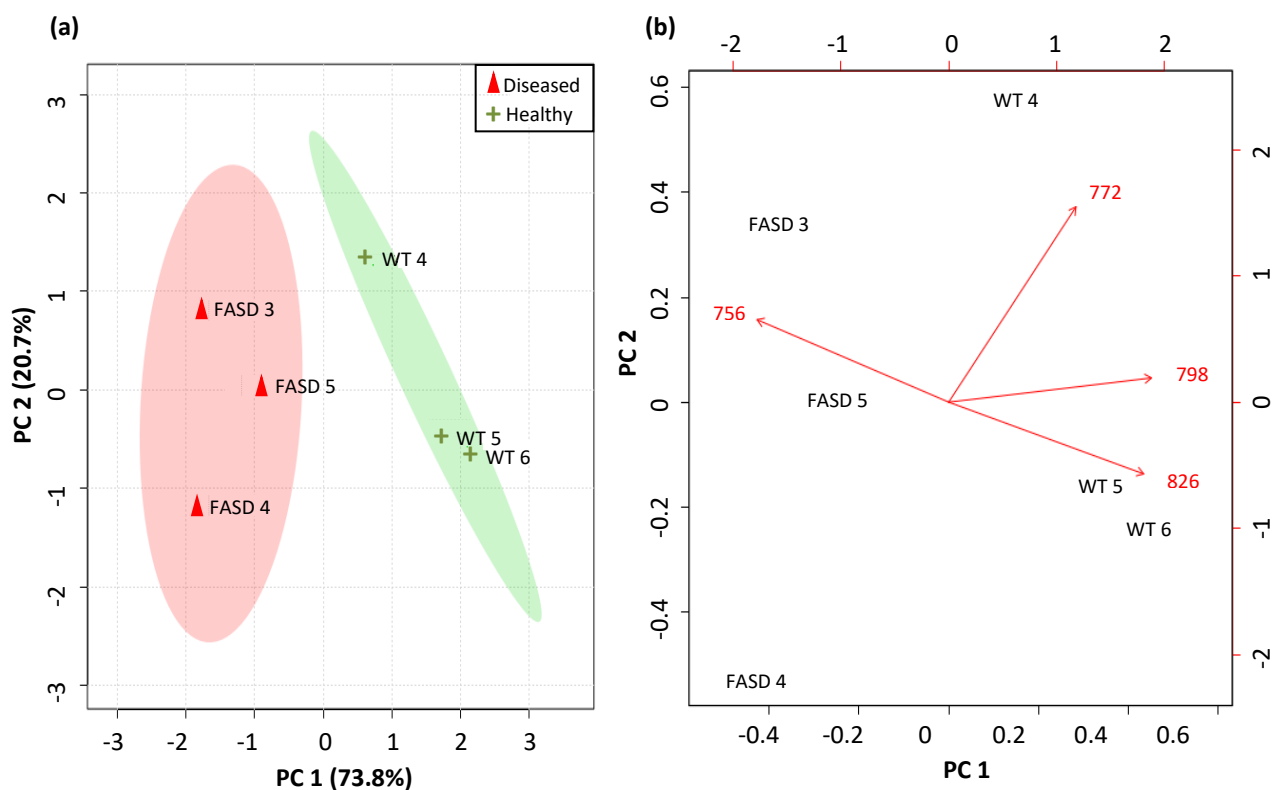


Figure 18: Principal Component Analysis of gray matter ROI in FASD (pink) and healthy (green) tissue samples in positive ionization mode. Principal component 1 and 2 (PC1 and PC2) corresponding to 73.8% and 20.7% variability in the data set were plotted on x-axis and y-axis respectively. The dataset was normalized to the base peak at m/z 782. (a) PCA score plot exhibit objects associated with average mass spectrum obtained from respective ROI of each sample. (b) PCA biplot shows contribution of different phospholipid ions in the gray matter of FASD and healthy mouse brain samples. The ion at m/z 756 formed acute angle with FASD cluster and was consequently more abundant in gray matter of FASD brains. All other ions formed acute angle with the wildtype cluster and were consequently more abundant in the gray matter of healthy brains.

PCA analysis of entire FASD and control brains demonstrated higher abundance of sodium adduct of PC(16:0/18:1) at m/z 782 in FASD brain as opposed to the control (Figure 15b). Furthermore, the signal intensity of this ion was higher in the gray matter of healthy brain in comparison to its white matter (Figure 17b). On the other hand, its relative abundance was 100% in FASD brain due to which it was used to normalize the data set. Consequently, it could not be used to compare FASD gray and white matter (Figure 16 a,b) as well as to compare the gray matter of FASD and healthy brains (Figure 18 a,b) indicating that it is predominantly distributed in the gray matter of FASD brain. PCA analysis of white matter of FASD and wildtype brains indicated higher abundance in FASD brain as opposed to healthy (Figure 19b). Consequently, these results demonstrate that alcohol does not impact the distribution of PC (16:0/18:1) but solely increases its abundance in FASD mouse models.

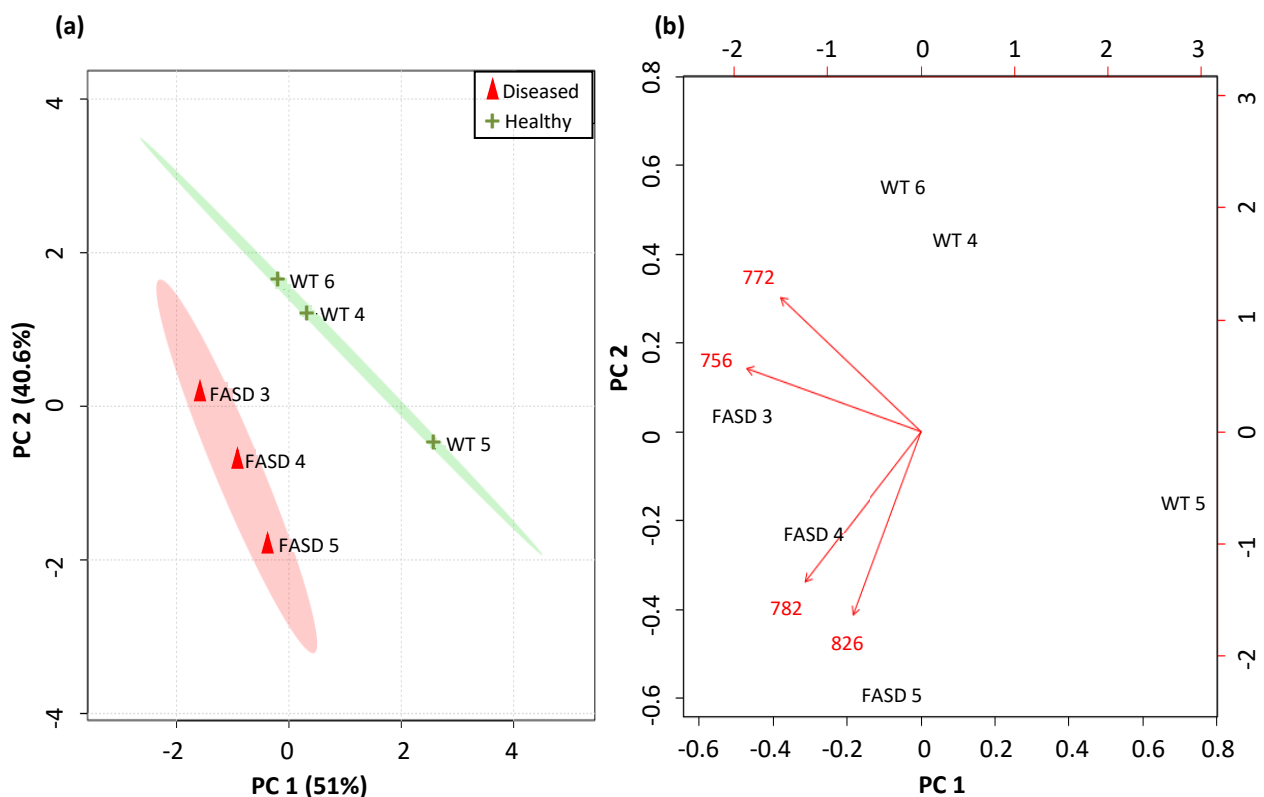


Figure 19: Principal Component Analysis of ROI corresponding to white matter of FASD (pink) and healthy (green) brain samples in positive ionization mode. Principal component 1 and 2 (PC1 and PC2) corresponding to 51% and 40.6% variability in the data set were plotted on x-axis and y-axis respectively. The dataset was normalized to the base peak at m/z 798. (a) PCA score plot include objects representing average mass spectrum obtained from white matter ROI of each sample. (b) PCA biplot indicating the formation of acute angle of all ions with FASD cluster.

The signal intensity of ion at m/z 798 corresponding to potassium adduct of PC(16:0/18:1) and sodium adduct of PE(P-18:0/22:6) was maximum in both FASD and healthy brains; as a result, it was used to normalize the data set for PCA analysis of whole brains (Figure 15 a,b), gray and white matter of healthy brain (Figure 17 a,b), and white matter of healthy and FASD brain (Figure 19 a,b). PCA analysis of gray and white matter of FASD brain illustrated higher abundance in white matter (Figure 16b); while PCA analysis of healthy and FASD gray matter suggested higher abundance in wildtype as opposed to FASD (Figure 18b). These results indicate that phosphatidylcholine and phosphatidylethanolamine are more abundant in wildtype than FASD brain and are relatively higher in white matter of the brain as compared to the gray matter. Majority of the phosphatidylcholine species demonstrated significantly higher level in FASD afflicted mice. The Enhanced level of phosphatidylcholine and acetylcholine has been linked with depression and anxiety like symptoms in other diseases which are also detected in FASD patients.²⁶

The PCA analysis of potassium adduct of PC(18:0/18:1) at m/z 826 illustrated higher abundance in the entire healthy brain as opposed to FASD (Figure 15b). Furthermore, this ion was predominantly distributed in the white matter of both wildtype and FASD brains (Figure 16b, 17b). The PCA analysis of healthy and FASD gray matter indicated higher abundance in healthy brain (Figure 18b). However, PCA analysis of healthy and FASD white matter demonstrated higher abundance in FASD brain as compared to healthy (Figure 18b). Thus, alcohol reduces the overall abundance of PC(18:0/18:1) in the brain and imposes relatively greater impact on the gray matter than the white matter of the brain. Lower abundance of PC (18:0/18:1) might be associated with its lower turnover rate in white matter in comparison to other phosphatidylcholine species localized in gray matter of the brain.⁷⁹

3.3.2 Principal Component Analysis in Negative Ionization Mode

A similar trend was observed for PCA analysis performed in the negative ionization mode with selection criteria of 5-8% and 25% relative intensity threshold that was normalized to the base peak at m/z 834. Lower threshold criterion contributing to the large number of

phospholipids could not separate FASD and wildtype samples in PCA score plot; while higher threshold criterion associated with 5 major ions of interest successfully separated the two sample sets (Figure 20a). PCA analysis was conducted on the entire FASD and healthy brains (Figure 20 a,b); gray and white matter of wildtype brain (Figure 21 a,b); gray and white matter of FASD brain (Figure 22 a,b); gray matter of FASD and wildtype brain (Figure 23 a,b); and white matter of FASD and wildtype brain (Figure 24 a,b).

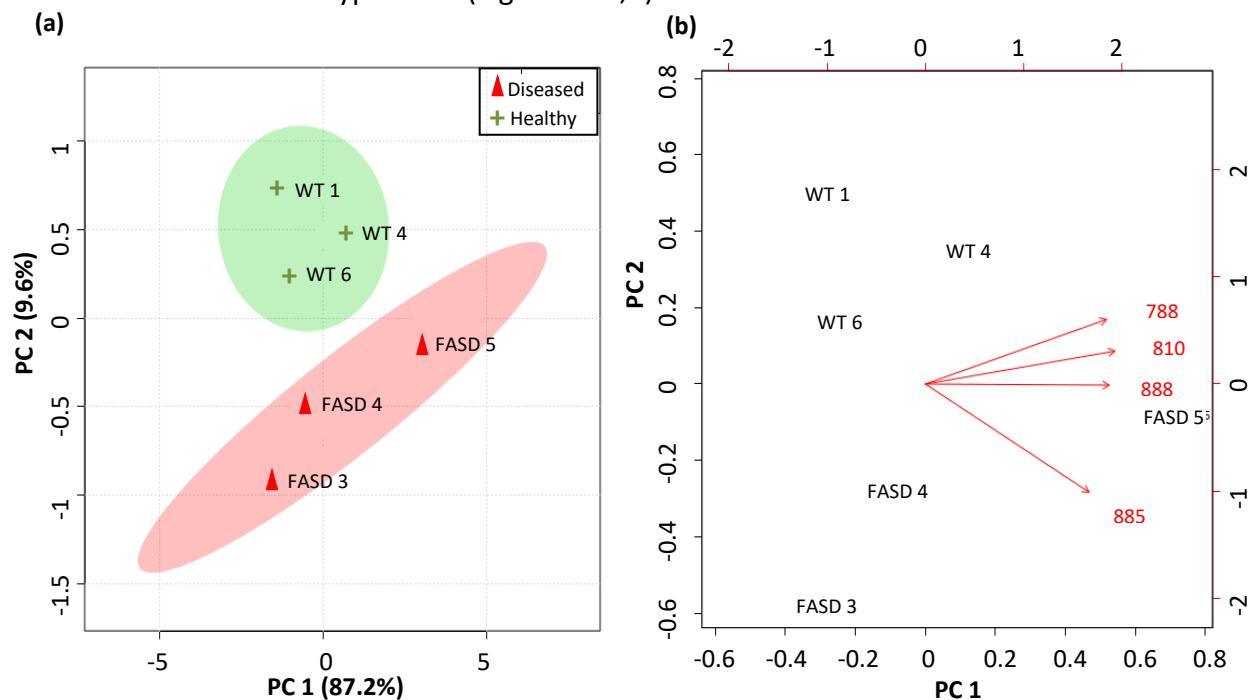


Figure 20: Principal Component Analysis of FASD samples in negative ionization mode. Six mice samples comprising three wildtype (green) and three FASD (pink) brain tissues were subjected to PCA analysis. PCA analysis was computed using entire brain area selected as the region of interest. Principal component 1 and 2 (PC1 and PC2) corresponding to 87.2% and 9.6% variability in the data set were plotted on x-axis and y-axis respectively. The dataset was normalized to the base peak at m/z 834. (a) PCA score plot shows wildtype and FASD objects corresponding to the average mass spectrum obtained from whole brain ROI of each sample. (b) PCA biplot indicates contribution of 5 major phospholipid ions in the separation of FASD and wildtype tissue samples. All the ions formed acute angle with FASD cluster and were consequently more abundant in the entire FASD brain in comparison to the healthy brain.

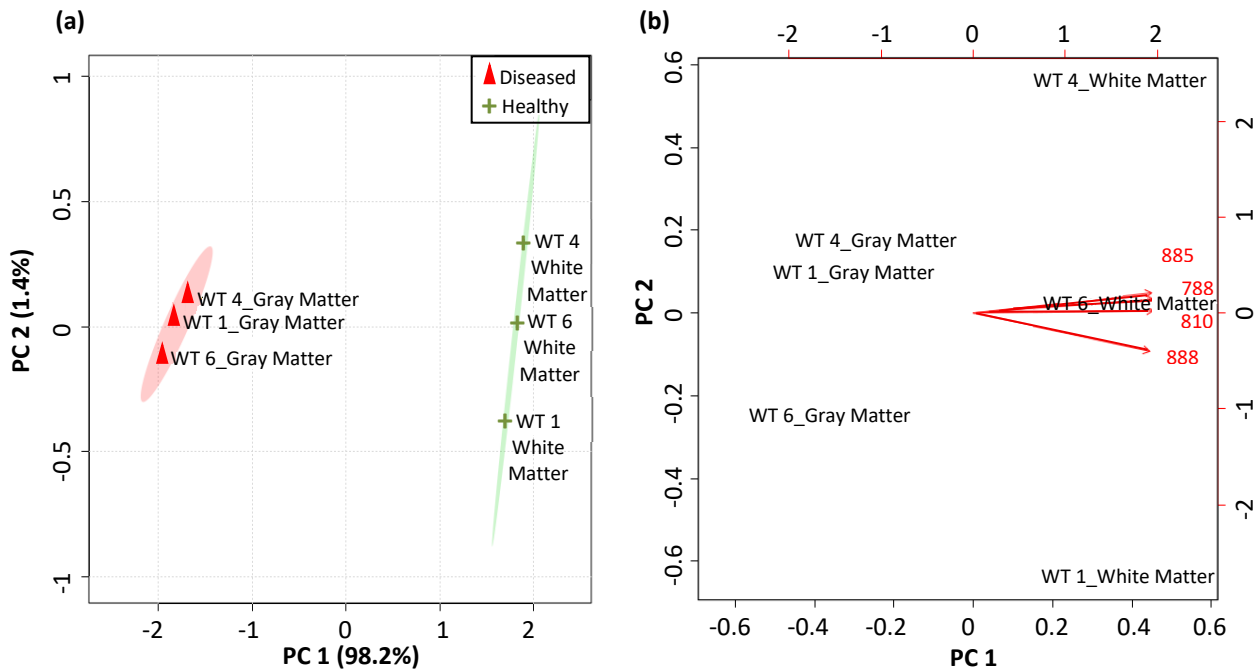


Figure 21: Principal Component Analysis of wildtype samples in negative ionization mode. PCA analysis was performed on region of interest corresponding to gray (pink) and white (green) matter of healthy brain. Principal component 1 and 2 (PC1 and PC2) corresponding to 98.2% and 2.4% variability in the data set were plotted on x-axis and y-axis respectively. The dataset was normalized to the base peak at m/z 834. (a) PCA score plot include points representing average mass spectrum of each sample obtained from its respective ROI. (b) PCA biplot shows contribution of different phospholipid ions in the separation of gray and white matter of healthy mouse brain samples. All the ions formed acute angle with the cluster of white matter and were consequently more abundant in the white matter of healthy brains.

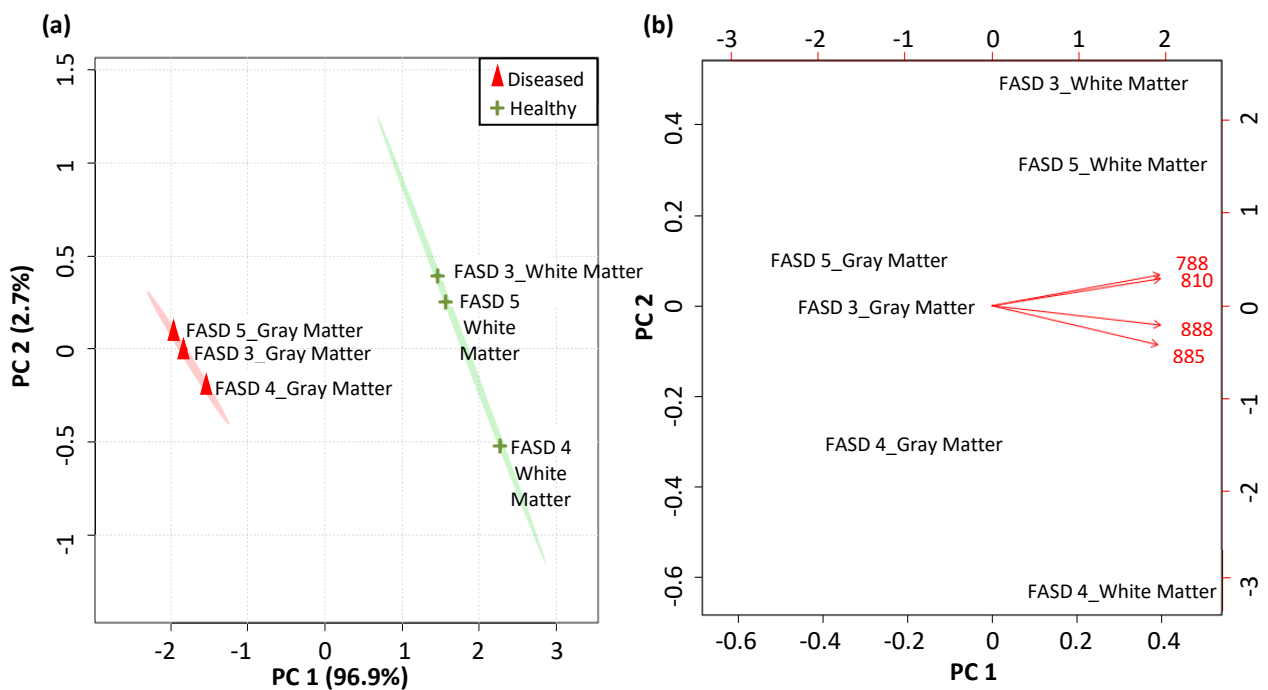


Figure 22: Principal Component Analysis of FASD samples in negative ionization mode. PCA analysis was conducted on gray (pink) and white (green) matter ROI. Principal component 1 and 2 (PC1 and PC2) corresponding to 96.9% and 2.7% variability in the data set were plotted on x-axis and y-axis respectively. The dataset was normalized to the base peak at m/z 834. (a) PCA score plot include objects depicting average mass spectrum obtained from respective ROI of each sample. (b) PCA biplot indicates contribution of various phospholipid ions in the separation of gray and white matter of FASD tissue samples. All the ions formed acute angle with the cluster of white matter and were consequently more abundant in the white matter of FASD brains.

PS(18:0/18:0), PS(18:0/20:0), and PS(18:0/22:6) were more abundant in entire FASD brain (Figure 13d) as well as in the gray and white matter of FASD brain as opposed to healthy brain as illustrated in Figure 23b, and 24b. The PCA analysis of gray and white matter of FASD brain; and gray and white matter of healthy brain showed greater profusion of PS in the white matter of both FASD and healthy subjects suggesting that PS is primarily localized in the white matter of the brain. These results indicate that alcohol increases the abundance of PS in FASD mouse models but does not impact its localization within the brain. Higher abundance of PS has been linked with neurodegeneration in various diseased states which might be the case in FASD mouse models as well.³⁶

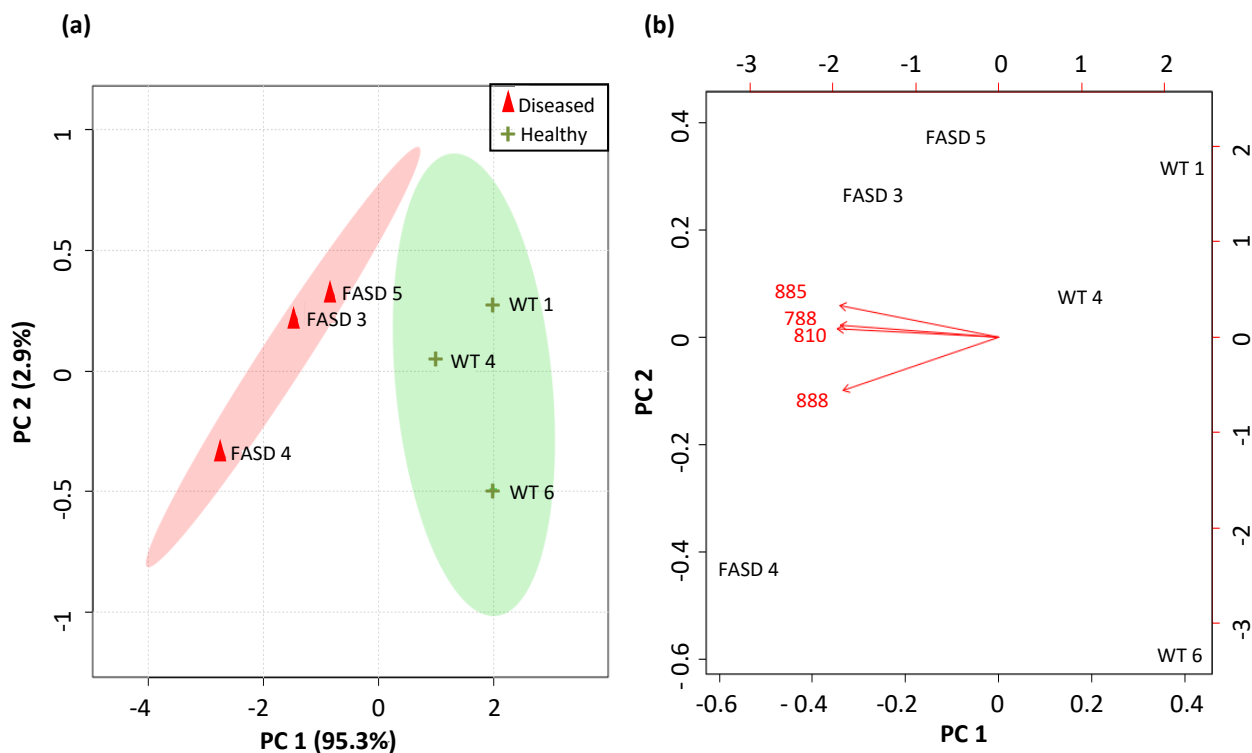


Figure 23: Principal Component Analysis of ROI corresponding to gray matter of FASD (pink) and healthy (green) tissue samples in negative ionization mode. Principal component 1 and 2 (PC1 and PC2) corresponding to 95.3% and 2.9% variability in the data set were plotted on x-axis and y-axis respectively. The dataset was normalized to the base peak at m/z 834. (a) PCA score plot exhibit objects associated with average mass spectrum obtained from respective ROI of each sample. (b) PCA biplot shows contribution of different phospholipid ions in the gray matter of FASD and healthy mouse brain samples. All the ions formed acute angle with the FASD cluster and were consequently more abundant in the gray matter of FASD brains.

The PCA analysis of PI(18:0/20:4) at m/z 885 showed a similar trend as PS with higher abundance in the entire FASD brain as well as FASD gray and white matter in comparison to entire healthy brain, and gray and white matter of health brain respectively (Figure 20b, 23b, 24b). Furthermore, biplot of wildtype gray and white matter indicated higher intensity of PI in white matter of the brain (Figure 21b). Similarly, biplot of FASD gray and white matter illustrated higher intensity of PI in white matter of FASD brain (Figure 22b). These results demonstrate that alcohol exclusively enhances the relative abundance of PI(18:0/20:4) in FASD brain without imposing any impact on its distribution within the brain. Higher concentration of phosphatidylinositol might be detrimental for the brain development as it can overstimulate large number of cellular pathways mediated by PI and its phosphorylated products causing adverse effects related to brain development in FASD patients.³⁹

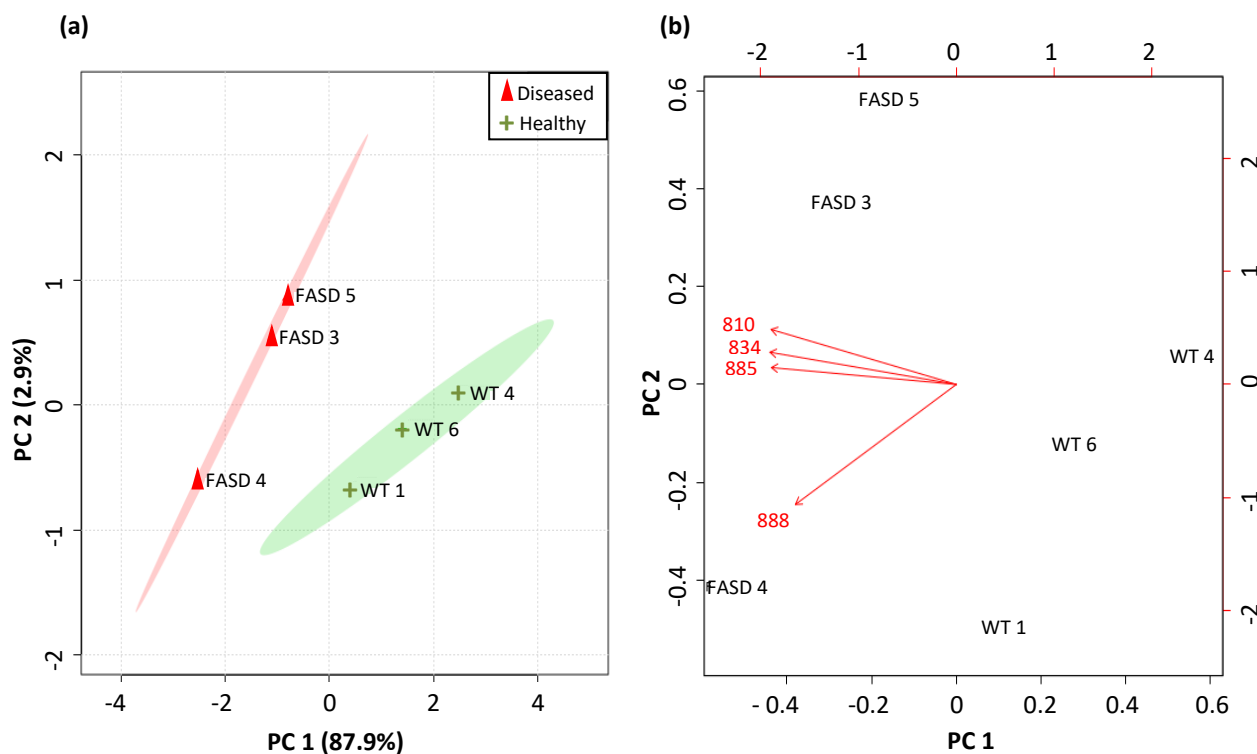


Figure 24: Principal Component Analysis of ROI corresponding to white matter of FASD (pink) and healthy (green) brain samples in negative ionization mode. Principal component 1 and 2 (PC1 and PC2) corresponding to 87.9% and 9.6% variability in the data set were plotted on x-axis and y-axis respectively. The dataset was normalized to the base peak at m/z 788. (a) PCA score plot include objects representing average mass spectrum obtained from white matter ROI of each sample. (b) PCA biplot shows contribution of various phospholipid ions in the white matter of FASD and wildtype samples. All the ions formed acute angle with the FASD cluster and were consequently more abundant in the white matter of FASD brains.

The signal intensity of ion at m/z 888 corresponding to ST(24:1) was higher in the entire FASD brain as compared to healthy brain (Figure 20b). Its abundance was also higher in the gray and white matter of FASD brain in comparison to the gray and white matter of healthy brain (Figure 23, 24). Furthermore, PCA analysis of gray matter and white matter in healthy brain indicated higher relative intensity of ST in the white matter (Figure 21b). A similar trend was observed in the PCA analysis of gray and white matter of FASD brain with higher abundance in white matter as opposed to the gray matter of the brain (Figure 22b). These results demonstrate that alcohol increases the accumulation of ST(24:1) in FASD brain and primarily localizes sulfatide in white matter of the brain. Higher sulfatide levels have been associated with demyelination that might also lead to impairments in brain development of FASD subjects.⁴⁷

PCA analysis served as an essential tool to validate the results acquired in DESI-MS images and to explore the extent of variability in phospholipid ion intensities of wildtype and FASD samples. PCA analysis demonstrated distinct clusters of gray and white matter in wildtype and FASD brain indicating that all regions of the brain were highly impacted by alcohol administration in FASD mouse models. The phospholipid profile was not only different for various regions within the FASD brain but it was considerably different from the gray and white matter of wildtype brain as well. DESI-MS images and PCA biplot demonstrated enhanced level of PC(16:0/16:0) and PC (16:0/18:1) in both gray and white matter of the brain in response to alcohol. While, the level of PE(P-16:0/22:6), PS(18:0/18:1), PS(18:0/20:0) and ST(24:1) increased specifically in the white matter of FASD brain as illustrated by both DESI-MS images and PCA biplot. DESI-MS images represented homogenous distribution of PC(16:0/18:1), PE(P-

18:0/22:6), PS(18:0/22:6) and PI(18:0/20:4) in the brain; while it could not demonstrate the impact of alcohol on the level of these phospholipids. On the other hand, biplot of PCA analysis revealed that these phospholipids were relatively more abundant in the white matter of the brain instead of being homogeneously distributed throughout the brain. Furthermore, consumption of alcohol was shown to reduce the level of PC(16:0/18:1) and PE(P-18:0/22:6); while enhance the level of PS(18:0/22:6) and PI(18:0/20:4) in the brain. Lastly, PCA biplot and DESI-MS images illustrated reduced level of PC(18:0/18:1) in response to alcohol consumption in FASD brain samples. All these phospholipids play distinct roles in neuronal differentiation and survival. Variations in phospholipid levels can drastically hinder cell proliferation, trigger transmigration of lipids within the bilayer, disrupt neuronal signal transmission, alter neurotransmitter levels, induce apoptotic effects and initiate neuronal degeneration in the brain. These destructive effects are significantly more pronounced in developing brain undergoing extensive neuronal differentiation as in the case of FASD in comparison to a well-developed brain of an adult.

CHAPTER IV

Conclusion and Future Work

Mass spectrometry has been widely used to investigate oxidative and non-oxidative alcohol metabolic products and alterations of embryonic proteins in FASD subjects. This work highlights the application of ambient mass spectrometry imaging, specifically DESI-MSI, in evaluating the impact of alcohol on phospholipids of developing fetal brain. DESI-MS images depicted a distinct variation in the relative abundance of phospholipids and their distribution in various regions of the brain. Multiple replicates were conducted to validate the results and perform principal component analysis that served as a powerful tool for multivariate statistical analysis. PCA revealed significantly greater information regarding phospholipid distribution as opposed to information perceived from direct visualization of DESI-MS images. Remarkable disparity was detected in ten different phospholipids among which majority of the phospholipids demonstrated higher relative abundance in FASD brain. Furthermore, distinct distribution of phospholipids were detected in gray and white matter such that PC(18:0/18:1), PS(18:0/18:1), PS(18:0/22:6), and ST(24:1) were predominantly located in the white matter of the brain while all other phospholipids were either dispersed throughout the brain or distributed primarily in the gray matter of the brain. DESI-MS integrated with statistical analysis demonstrates great potential for forensic studies on human patients suffering from FASD disease due to its ability of substantially differentiating normal and FASD tissue samples.

This work serves as an essential preliminary study that lays a strong foundation for understanding biological relevance and impact of phospholipid variation on cell proliferation and signalling pathways in developing fetal brain. However, it primarily focused on 10 phospholipids that were detected by DESI and could not explore the entire range of phospholipids in a lipidomic study of the fetal brain. Furthermore, it was limited to relative quantification of phospholipids in various regions of the brain instead of absolute quantification which can reveal significantly greater information regarding the alteration in the abundance of these phospholipids in response to alcohol. Consequently, the research can be extended to

further investigate these phospholipids using LC-MS based methods as lipid extraction from the entire fetal brain followed by separation of these phospholipids by liquid chromatography would allow the detection of large number of phospholipids there were not previously detected by DESI. Furthermore, addition of labeled internal standards in the lipid extract would allow absolute quantification of these phospholipids which would be of great interest for understanding biological mechanisms behind the variation of phospholipid abundance in patients suffering from fetal alcohol spectrum disorder.

REFERENCES

- [1] P. A. May, D. Fiorentino, G. Coriale, W. O. Kalberg, H. E. Hoyme, A. S. Aragón, D. Buckley, C. Stellavato, J. P. Gossage, L. K. Robinson, K. L. Jones, M. Manning, M. Ceccanti. *Int J Environ Res. Public Health* **2011**, 8: 2331-2351.
- [2] P. S. Brocardo, J. Gil-Mohapel, B. R. Christie. *Brain Res Rev.* **2011**, 67: 209-225.
- [3] J. Stiles, T. L. Jernigan. *Neuropsychol Rev.* **2010**, 20: 327-348.
- [4] N. Dorrie, M. Focker, I. Freunsch, J. Hebebrand. *Eur Child Adolesc Psychiatry* **2014**, 23: 863-875.
- [5] W. A. Chen, S. E. Maier, S. E. Parnell, J. R. West. *Alcohol Res Health* **2003**, 27: 174-180.
- [6] A. L. Norman, N. Crocker, S. N. Mattson, E. P. Riley. *Dev Disabil Res Rev.* **2009**, 15: 209-217.
- [7] L. A. Leigland, M. M. Ford, J. P. Lerch, C. D. Kroenke. *Alcohol Clin Exp Res.* **2013**, 37: 924-932.
- [8] L. M. Squeglia, J. Jacobus, S. F. Tapert. *Handb Clin Neurol.* **2014**, 125: 501-510.
- [9] M. Patra, E. Salonen, E. Terama, I. Vattulainen, R. Faller, B. W. Lee, J. Holopainen, M. Karttunen. *Biophys J.* **2006**, 90: 1121-1135.
- [10] J. K. Young, H. E. Giesbrecht, M. N. Eskin, M. Aliani, M. Suh. *Adv Nutr.* **2014**, 5: 675-692.
- [11] C. F. Bearer, S. Gould, R. Emerson, P. Kinnunen, C. S. Cook. *Pediatr Res.* **1992**, 31: 492-495.
- [12] D. W. Clarke, G. N. Smith, J. Patrick, B. Richardson, J. F. Brien. *Dev Pharmacol Ther.* **1989**, 12: 35-41.
- [13] M. Tong, L. Longato, Q. Nguyen, W. C. Chen, A. Spaisman, S. M. de laMonte. *Oxid Med Cell Longev.* **2011**, 1-13.
- [14] J. Chanda, S. Bandyopadhyay. *Langmuir* **2006**, 22: 3775-3781.
- [15] R. R. M. Jr, E. J. Touney, W. J. Vandivier, F. J. Raymond. *Comp Biochem Physiol.* **1998**, 120: 91-98.
- [16] J. A. Hernández, R. C. López-Sánchez, A. Rendón-Ramírez. *Oxid Med Cell Longev.* **2016**, 1-15.
- [17] L. Gustavsson. *Alcohol Alcoholism.* **1995**, 30: 391-406.
- [18] J. Bai, T. L. H. Trinh, K. Chuang, A. Qiu. *Magnetic Resonance Imaging.* **2012**, 30: 789-798.
- [19] M. Wright, W. Skaggs, F. Å. Nielsen. *WikiJournal of Medicine.* **2016**, 3: 1-15.

- [20] E. Mooshagian. *The Journal of Neuroscience*. **2008**, 28: 1535–1536.
- [21] D. Amaral, P. Lavenex. *New York: Oxford University Press*. **2007**, p. 37.
- [22] E. Stellar. *Psychological Review*. **1994**, 101: 301-311.
- [23] M. S. Gazzaniga, R. B. Ivry, G. R. Mangun. *New York: W.W. Norton*. **2014**, p. 45.
- [24] J. K. Chilton. *Dev Biol*. **2006**, 292 (1): 13-24
- [25] L. Paoletti, C. Elena, P. Domizi, C. Banchio. *IUBMB Life*. **2011**, 63 (9): 714-720.
- [26] H. Kadowaki, M. A. Grant. *J Lipid Res*. **1995**, 36: 1274-1282.
- [27] J. K. Blusztajn, M. Liscovitch, C. Mauron, U. I. Richardson, R. J. Wurtman. *J Neural Transm Suppl*. **1987**, 24: 247-289.
- [28] S. Y. Chung, T. Moriyama, E. Uezu, K. Uezu, R. Hirata, N. Yohena, Y. Masuda, T. Kokubu, S. Yamamoto. *J Nutr*. **1995**, 125(6): 1484-1489.
- [29] S. MacKay, D. J. Meyerhoff, J. Constans, D. Norman, G. Fein, M. W. Weiner. *Arch Neurol*. **1996**, 53(2): 167-174.
- [30] M. J. Higley, M. R. Picciotto. *Curr Opin Neurobiol*. **2014**, 0: 88-95.
- [31] A. Adeyinka, N. P. Kondamudi. *StatPearls Publishing LLC*. Book. **2018**.
- [32] Y. S. Mineur, A. Obayemi, M. B. Wiggestrand, G. M. Fote, C. A. Calarco, A. M. Li, M. R. Picciotto. *Proc Natl Acad Sci*. **2013**, 110(9): 3573-3578.
- [33] A. D. Purdon, S. I. Rapoport. *Biochem J*. **1998**, 335: 313-318.
- [34] R. Kakela, P. Somerharju, J. Tynnela. *J Neurochem*. **2003**, 84: 1051-1065.
- [35] R. F. A. Zwaal, P. Comfurius, E. M. Bevers. *Cell Mol Life Sci*. **2005**, 62: 971-988.
- [36] Y. E. Kim, J. Chen, R. Langen, J. R. Chan. *Nat Protoc*. **2010**, 5(8): 1396-1405.
- [37] H. Kim, B. X. Huang, A. A. Spector. *Prog Lipid Res*. **2014**, 0: 1-18.
- [38] R. F. Irvine. *J Lipid Res*. **2016**, 57:1987-1994.
- [39] Y. Muftuoglu, Y. Xue, X. Gao, D. Wu, Y. Ha. *Proc Natl Acad Sci*. **2016**, 113(31): 8711-8716.
- [40] G. D. Paolo, P. D. Camilli. *Nature*. **2006**, 443(7112): 651-657.
- [41] D. Kong, T. Yamori. *Cancer Sci*. **2008**, 99(9): 1734-1740.
- [42] J. L. Dupree, K. Suzuki, B. Popko. *Microsc Res Techniq*. **1998**, 41(5): 431-440.
- [43] T. Takahashi, T. Suzuki. *J Lipid Res*. **2012**, 53(8): 1437-1450.
- [44] R. Bansal, S. E. Pfeiffer. *Proc Natl Acad Sci*. **1989**, 86: 6181-6185.
- [45] T. Ishibashi, J. L. Dupree, K. Ikenaka, Y. Hirahara, K. Honke, E. Peles, B. Popko, K. Suzuki, H. Nishino, H. Baba. *J Neurosci*. **2002**, 22(15): 6507-6514.

- [46] R. Bansal, S. Winkler, S. Bheddah. *J Neurosci.* **1999**, 19(18):7913-7924.
- [47] H. Ramakrishnan, K. K. Hedayati, R. Lullmann-Rauch, C. Wessig, S. N. Fewou, H. Maier, H. Goebel, V. Gieselmann, M. Eckhardt. *J Neurosci.* **2007**, 27(35): 9482-9490.
- [48] M. Eckhardt, K. K. Hedayati, J. Pitsch, R. Lullmann-Rauch, H. Beck, S. N. Fewou, V. Gieselmann. *J Neurosci.* **2007**, 27(34): 9009-9021.
- [49] N. Fabelo, V. Martín, G. Santpere, R. Marín, L. Torrent, I. Ferrer, M. Díaz. *Mol Med.* **2011**, 17(9):1107-1118.
- [50] R. V. Zyl, V. Gieselmann, M. Eckhardt. *J Neurochem.* **2010**, 112:282-295.
- [51] M. Roehsig, D. M. L. de Paula, S. Moura, E. M. de A. Diniz, M. Yonamine. *J Sep Sci.* **2010**, 33, 2115-2122.
- [52] P. Cabarcos, M. J. Taberner, I. Álvarez, M. Miguez, P. Fernández, A. M. Bermejo. *Anal Bioanal Chem.* **2012**, 404, 147-155.
- [53] S. Pichini, M. Pellegrini, J. Gareri, G. Koren, O. Garcia-Algar, O. Vall, F. Vagnarelli, P. Zuccaro, E. Marchei. *J Pharmaceut Biomed.* **2008**, 48, 927-933.
- [54] L. N. Bakhireva, D. D. Savage. *Alcohol Res Health.* **2011**, 34, 56-63.
- [55] S. Wang, R. Yang, F. Ji, H. Li, J. Dong, W. Chen. *Talanta* **2017**, 166, 315-320.
- [56] K. L. Davis-Anderson, S. Berger, E. R. Lunde-Young, V. D. Naik, H. Seo, G. A. Johnson, H. Steen, J. Ramadoss. *Alcohol. Clin Exp Res.* **2017**, 41, 1551-1558.
- [57] S. Mason, B. Anthony, X. Lai, H. N. Ringham, M. Wang, F. A. Witzmann, J. You, F. C. Zhou. *Int J Proteom.* **2012**, 1-10.
- [58] J. Ramadoss, R. R. Magness. *Reprod Toxicol.* **2012**, 34, 538-544.
- [59] S. Datta, D. Turner, R. Singh, L. B. Ruest, W. M. Pierce Jr., T. B. Knudsen. *Birth Defects Res A Clin Mol Teratol.* **2008**, 82, 177-186.
- [60] C. J. Perez, A. K. Bagga, S. S. Prova, M. Yousefi Taemeh, D. R. Ifa. *Rapid Commun Mass Spectrom.* **2018**, 1-27.
- [61] Z. Takats, J. M. Wiseman, B. Gologan, R. G. Cooks. *Science* **2004**, 306, 471-473.
- [62] P. Vaysse, R. M. A. Heeren, T. Porta, B. Balluff. *Analyst* **2017**, 142, 2690-2712.
- [63] A. Venter, P. E. Sojka, R. G. Cooks. *Anal Chem.* **2006**, 78: 8549-8555.
- [64] Z. Takats, N. Strittmatter, J. S. McKenzie. *Adv Cancer Res.* **2017**, 134: 231-256.
- [65] L. S. Eberlin, C. R. Ferreira, A. L. Dill, D. R. Ifa, R. G. Cooks. *Biochim Biophys Acta.* **2011**, 1811, 946-960.
- [66] C. Wu, A. L. Dill, L. S. Eberlin, R. G. Cooks, D. R. Ifa. *Mass Spectrom Rev.* **2013**, 32, 218-243.
- [67] Z. Takats, J. M. Wiseman, R. G. Cooks. *J Mass Spectrom.* **2005**, 40:1261-1275.

- [68] J. M. Wiseman, D. R. Iffa, A. Venter, R. G. Cooks. *Nat Protoc.* **2008**, 3(3): 517-524.
- [69] M. Shariatgorji, P. Svenningsson, P. E. Andren. *Neuropsychopharmacol.* **2014**, 39: 34-39.
- [70] S. Chapman, P. Schenk, K. Kazan, J. Manners. *Bioinformatics.* **2002**, 18(1): 202-204.
- [71] H. Abdi, L. J. Williams. *Computational Statistics.* 2010, 2(1): 433-459.
- [72] W. Yan, N. A. Tinker. *Can J Plant Sci.* **2006**, 86(3): 623-645.
- [73] G. C. Burdge, A. D. Postle. *Biochimica. et Biophysica. Acta.* **1995**, 1256, 346-352.
- [74] C. Lindi, G. Montorfano, F. Rossi, R. Gornati, A. M. Rizzo. *Alcohol Alcoholism* **2001**, 36, 388-392.
- [75] A. D. Postle, D. C. Wilton, A. N. Hunt, G. S. Attard. *Prog. Lipid Res.* **2007**, 46, 200-224.
- [76] A. Reis, A. Rudnitskaya, G. J. Blackburn, N. M. Fauzi, A. R. Pitt, C. M. Spickett. *J. Lipid Res.* **2013**, 54, 1812-1824.
- [77] J. Xia, N. Psychogios, N. Young, D. S. Wishart. *Nucleic Acids Res.* **2009**, 37: 652-660.
- [78] R. A. van den Berg, H. C. J. Hoefsloot, J. A. Westerhuis, A. K. Smilde, M. J. van der Werf. *BMC Genomics.* **2006**, 7:142
- [79] A. H. Ousley, P. Morell. *J Biol Chem.* **1992**, 267(15): 10362-10369.